

13 Eliashberg Theory

Giovanni A.C. Ummarino

Departement of Applied Science and Technology

Politecnico di Torino, 10129 Turin, Italy

Contents

1	Introduction	2
2	Imaginary-axis Eliashberg equations	5
2.1	Nambu formalism	5
2.2	Migdal-Eliashberg theory	6
2.3	Coulomb pseudopotential	10
3	Real-axis Eliashberg equations	11
4	Simplified approaches	12
4.1	BCS limit	12
4.2	Critical temperature	12
5	Relation between real- and imaginary-axis formulation	13
5.1	Padé method for analytic continuation	13
5.2	Marsiglio, Schossmann, and Carbotte formulation	15
6	Tunneling inversion of the standard Eliashberg equations	15
7	Approximations of the standard Eliashberg equations	18
8	Cuprate high-temperature superconductors	19
9	Multi-band Eliashberg theory	21
10	Iron pnictide superconductors	24
10.1	Gaps, critical temperature, and upper critical magnetic field	24
10.2	Interaction mechanism	31
11	Conclusion	32

1 Introduction

The first microscopic theory for superconductivity was proposed in 1957 by Bardeen, Cooper and Schrieffer [1] almost 50 years after the discovery of Kamerlingh Onnes of the zero electric resistance of the mercury below 4.1 K. The theory of superconductivity can be divided into two separate areas: first the establishment of a pairing formalism, which leads to a superconducting condensate, given some attractive particle-particle interaction, and secondly, a mechanism by which two electrons might attract one another. BCS [2], by simplifying the interaction, succeeded in establishing the pairing formalism. Indeed, one of the elegant outcomes of the BCS pairing formalism is the universality of various properties; at the same time this universality means that the theory really does not distinguish one superconductor from another, and, more seriously, one mechanism from another. Luckily, while many superconductors do display universality, some do not, and these, as it turns out, provide very strong support for the electron-phonon mechanism. Before one establishes a theory of superconductivity, one requires a satisfactory theory of the normal state [3]. In conventional superconductors, the Fermi liquid theory appears to work very well, so that, while we cannot solve the problem of electrons interacting through the Coulomb interaction, experiment tells us that Coulomb interactions give rise to well-defined quasiparticles, i.e., a set of excitations which are in one-to-one correspondence with those of the free-electron gas. The net result is that one begins the problem with a reduced Hamiltonian

$$H_{\text{red}} = \sum_{\mathbf{k}\sigma} \varepsilon_{\mathbf{k}} c_{\mathbf{k}\sigma}^\dagger c_{\mathbf{k}\sigma} + \sum_{\mathbf{k}\mathbf{k}'} V_{\mathbf{k},\mathbf{k}'} c_{\mathbf{k}\uparrow}^\dagger c_{-\mathbf{k}\downarrow}^\dagger c_{-\mathbf{k}'\downarrow} c_{\mathbf{k}'\uparrow}, \quad (1)$$

where, for example, the electron energy dispersion $\varepsilon_{\mathbf{k}}$ already contains much of the effect due to Coulomb interactions. The important point is that well-defined quasiparticles with a well defined energy dispersion near the Fermi surface are assumed to exist, and are summarized by the dispersion $\varepsilon_{\mathbf{k}}$ with a pairing interaction $V_{\mathbf{k},\mathbf{k}'} \equiv V(\mathbf{k}, \mathbf{k}')$. The BCS equations is

$$\Delta_{\mathbf{k}} = - \sum_{\mathbf{k}'} V_{\mathbf{k},\mathbf{k}'} \frac{\Delta_{\mathbf{k}'}}{2E_{\mathbf{k}'}} \tanh \frac{E_{\mathbf{k}'}}{2T}, \quad (2)$$

where

$$E_{\mathbf{k}} = \sqrt{\varepsilon_{\mathbf{k}}^2 + \Delta_{\mathbf{k}}^2} \quad (3)$$

is the quasiparticle energy in the superconducting state, $\Delta_{\mathbf{k}}$ the variational parameter used by BCS, $N(0)$ the normal density of states at the chemical potential E_F , which is set to zero. An additional equation which must be considered together with the gap equation is the number equation,

$$n = 1 - \frac{1}{N(0)} \sum_{\mathbf{k}'} \frac{\varepsilon_{\mathbf{k}'}}{E_{\mathbf{k}'}} \tanh \frac{E_{\mathbf{k}'}}{2T}. \quad (4)$$

Given a pair potential and an electron density, one has to solve these equations to determine the variational parameter $\Delta_{\mathbf{k}}$ and the chemical potential, generally with an iterative numerical method. For conventional superconductors the chemical potential hardly changes from the

normal to the superconducting state, and the variational parameter is much smaller than the chemical potential, with the result that the second equation was usually ignored. BCS then modeled the pairing interaction as a negative (and therefore attractive) constant potential V with a sharp cutoff in momentum space at the Debye energy ω_D

$$V_{\mathbf{k},\mathbf{k}'} \approx -V \theta(\omega_D - |\varepsilon_{\mathbf{k}}|) \theta(\omega_D - |\varepsilon_{\mathbf{k}'}|). \quad (5)$$

Using this potential in the BCS equation (2) with (3), along with a constant density of states assumption over the entire range of integration,

$$\frac{1}{\lambda} = \int_0^{\omega_D} \frac{\tanh(E/2T)}{E} d\varepsilon \quad (6)$$

where $\lambda = N(0)V$. At $T = 0$ K, the integral can be done analytically to give

$$\Delta = 2\omega_D \frac{\exp(-1/\lambda)}{1 - \exp(-1/\lambda)}. \quad (7)$$

Close to the critical temperature, T_c , the BCS equation becomes

$$\frac{1}{\lambda} = \int_0^{\omega_D/2T_c} \frac{\tanh x}{x} dx \quad (8)$$

which cannot be solved in terms of elementary functions for arbitrary coupling strength. Nonetheless, in weak coupling, one obtains

$$T_c = 1.13 \omega_D \exp(-1/\lambda). \quad (9)$$

It is clear that T_c or the zero temperature variational parameter Δ depends on material properties such as the phonon spectrum ω_D , the electronic structure $N(0)$ and the electron-ion coupling strength V . However, it is possible to form various thermodynamic ratios, that turn out to be independent of material parameters. The obvious example from the preceding equations is the ratio $2\Delta/T_c$. In weak coupling (most relevant for conventional superconductors), for example,

$$\frac{2\Delta}{T_c} = 3.53, \quad (10)$$

that is a universal result, independent of the material involved. Many other such ratios can be determined within BCS theory, and the observed deviations from these universal values contributed to the need for an improved formulation of BCS theory.

In the '60s the first discrepancies between the experimental results and the theoretical predictions began to be observed and the BCS theory [2] turned out to be inadequate for superconductors in which the electron-phonon interaction is strong. A primary reason for this is the instantaneous nature of the BCS interaction which does not incorporate enough of the physics of the electron-phonon system. For example, the electron-phonon interaction causes a mass

	$2\Delta/T_c$	$(C_s - C_n)/C_s$	λ	T_C
Al	3.535	1.43	0.43	1.18
Sn	3.705	1.68	2.77	3.75
Pb	4.497	2.77	1.55	7.22
Hg	4.591	2.49	1.62	4.19

Table 1: Deviations from the universality of BCS theory for some elemental superconductors.

enhancement of electron states near the Fermi level, seen in the specific heat, and a finite lifetime of electron quasiparticle states. In many material these effects are really, strong and well-defined quasiparticles no longer exists. Nevertheless, Migdal [4] showed that Feynman-Dyson perturbation theory can solve the electron-phonon problem to high accuracy, because the small parameter $\lambda\Omega_D/E_F \approx 10^{-3}$ keeps higher order corrections small.

Table 1 shows the values of the principal quantities for some characteristic elements. They differ more and more from the BCS predictions as the of coupling constant λ increases. According to BCS theory, the expected values are $2\Delta/T_C = 3.53$ and $(C_s - C_n)/C_s = 1.43$. These deviations arise when the interaction between electrons and phonons is strong, while in the weak-coupling approximation the properties of the lattice and the dispersion of phonon curves do not enter directly into the BCS theory.

The prediction of superconducting properties such as the critical temperature or the superconducting energy gap remains one of the outstanding challenges in modern condensed matter theory. Owing to the complex nature of the superconducting state, a quantitative understanding of the pairing mechanism in superconductors requires a very detailed knowledge of the electronic structure, the phonon dispersions, and the interaction between electrons and phonons. For example, in conventional superconductors below the critical temperature electron pairing results from a subtle interplay between the repulsive Coulomb interaction and the attractive electron-phonon interaction. Starting from the BCS theory several approaches to the calculation of the superconducting properties have been proposed for arriving at first-principles Green's function methods such as the Migdal-Eliashberg [5] formalism that provides a very accurate description of the superconducting state in almost all superconductors.

The electron-phonon coupling provided by Eliashberg theory is local in space and retarded in time, reflecting the delay in the development of lattice overscreening. The result is in contrast to the non local, instantaneous nature of the BCS model interaction, attractive for any pair of electrons within the Debye energy ω_D of the Fermi surface. Eliashberg theory is valid only when $\lambda\omega_D/E_F (\simeq \sqrt{m^*/M}) \ll 1$, where E_F is the Fermi level. This is the range of Migdal's theorem.

Migdal [4] argued that all vertex corrections are $\mathcal{O}(\sqrt{m^*/M})$, where m^* is the electron effective mass and M the ion mass, compared to the bare vertex, and therefore can be ignored; this means that only single phonon scattering terms will contribute to the electronic self energy.

2 Imaginary-axis Eliashberg equations

2.1 Nambu formalism

The Fröhlich interaction is formally very similar to the electron-electron interaction via Coulomb forces, thus the mutual scattering of two electrons can be explained through the electron-phonon-electron interaction in the same way. But the phase transition to the superconducting state invalidates the perturbation theory developed for a metal in the normal state. However, in 1960, Nambu showed [6] how the formalism used in the normal state can be rewritten in such a way that the diagrams used to deal with the normal state are applicable also to the superconducting state. The inclusion of Coulomb interactions causes the electron-phonon interaction to be screened and this can constitute a considerable reduction.

In spite of the strong electron-phonon coupling, it remains true that phonon corrections to the electron-phonon vertex are small. In contrast, Coulombic corrections are not necessarily small, but are more or less constant factors, so they can be included in the coupling constant. In the Nambu formalism a 2-component spinor for the electron

$$\psi_{\mathbf{k}} = \begin{pmatrix} c_{\mathbf{k}\uparrow} \\ c_{-\mathbf{k}\downarrow}^\dagger \end{pmatrix}, \quad \psi_{\mathbf{k}}^\dagger = \begin{pmatrix} c_{\mathbf{k}\uparrow}^\dagger & c_{-\mathbf{k}\downarrow} \end{pmatrix} \quad (11)$$

and a bare-phonon field operator

$$\varphi_{q\nu} = b_{q\nu} + b_{-q\nu}^\dagger \quad (12)$$

are defined. The Hamiltonian of an electron-phonon interacting system can be written [3] in terms of ψ and φ . Including Coulomb interactions and it becomes

$$\begin{aligned} H &= \sum_{\mathbf{k}} \varepsilon_{\mathbf{k}} \psi_{\mathbf{k}}^\dagger \varepsilon_{\mathbf{k}} \psi_{\mathbf{k}}^\dagger \sigma_3 \psi_{\mathbf{k}} + \sum_{q\lambda} \Omega_{q\lambda} b_{q\lambda}^\dagger b_{q\lambda} \sum_{\mathbf{k}\mathbf{k}'\lambda} g_{\mathbf{k},\mathbf{k}'\lambda} \varphi_{\mathbf{k}-\mathbf{k}'\lambda} \psi_{\mathbf{k}}^\dagger \sigma_3 \psi_{\mathbf{k}} \\ &+ \frac{1}{2} \sum_{\mathbf{k}_1\mathbf{k}_2\mathbf{k}_3\mathbf{k}_4} \langle \mathbf{k}_3\mathbf{k}_4 | V_C | \mathbf{k}_1\mathbf{k}_2 \rangle \left(\psi_{\mathbf{k}_3}^\dagger \sigma_3 \psi_{\mathbf{k}_1} \right) \left(\psi_{\mathbf{k}_4}^\dagger \sigma_3 \psi_{\mathbf{k}_2} \right), \end{aligned} \quad (13)$$

where $\varepsilon_{\mathbf{k}}$ is the one-electron Bloch energy relative to the Fermi level E_F , σ_3 is a Pauli matrix,¹ Ω is the bare phonon energy of wavevector \mathbf{q} and mode ν , $g_{\mathbf{k}\mathbf{k}'\nu}$ are electron phonon matrix elements, and V_C is the Coulomb potential.

Translational invariance of V_C restricts $\mathbf{k}_1 + \mathbf{k}_2 - \mathbf{k}_3 - \mathbf{k}_4$ to be either zero or a reciprocal lattice vector \mathbf{K} . The electrons are described in an extended zone scheme and the phonons are described in a reduced zone scheme which is extended periodically throughout \mathbf{q} -space. In order to apply perturbation methods to superconductors the possibility of the existence of Cooper pairs has to be included. This can be done taking the anomalous propagators. Using the

¹The Pauli matrices are

$$\sigma_1 = \begin{pmatrix} 0 & 1 \\ 1 & 0 \end{pmatrix}, \quad \sigma_2 = \begin{pmatrix} 0 & -i \\ i & 0 \end{pmatrix}, \quad \sigma_3 = \begin{pmatrix} 1 & 0 \\ 0 & -1 \end{pmatrix}$$

Nambu formalism the Green function [7] becomes

$$G(\mathbf{k}, \tau) = -\langle \mathcal{T} \{ \psi_{\mathbf{k}}(\tau) \psi_{\mathbf{k}}^\dagger(0) \} \rangle, \quad (14)$$

$$D_\lambda(\mathbf{q}, \tau) = -\langle \mathcal{T} \{ \varphi_{\mathbf{q}\lambda}(\tau) \varphi_{\mathbf{k}}^\dagger(0) \} \rangle \quad (15)$$

and the average is over the grand canonical ensemble ($\beta = 1/T$, where T is the temperature)

$$\langle Q \rangle = \frac{\text{Tr} e^{-\beta H} Q}{\text{Tr} e^{-\beta H}}, \quad (16)$$

where the operators evolve in imaginary time and \mathcal{T} is the time-ordering operator. As the matrix operator $\psi_{\mathbf{k}}(\tau) \psi_{\mathbf{k}}^\dagger(0)$ does not conserve the number of particles the definition of a new operator U that adjusts the number of particles is necessary:

$$U = 1 + R^\dagger + R, \quad (17)$$

where R converts a given state in an N -particle system into the corresponding state in the $N + 2$ particle system.

By this definition, the Green function for electrons is a 2×2 matrix, the diagonal elements are the conventional Green functions for spin-up electrons and spin-down holes, while G_{12} and G_{21} describe the pairing properties. It is defined as

$$G(\mathbf{k}, \tau) = - \begin{pmatrix} \langle \mathcal{T} \{ c_{\mathbf{k}\uparrow}(\tau) c_{\mathbf{k}\uparrow}^\dagger(0) \} \rangle & \langle U \mathcal{T} \{ c_{\mathbf{k}\uparrow}(\tau) c_{-\mathbf{k}\downarrow}(0) \} \rangle \\ \langle U \mathcal{T} \{ c_{-\mathbf{k}\downarrow}^\dagger(\tau) c_{\mathbf{k}\uparrow}^\dagger(0) \} \rangle & \langle \mathcal{T} \{ c_{-\mathbf{k}\downarrow}^\dagger(\tau) c_{-\mathbf{k}\downarrow}(0) \} \rangle \end{pmatrix}. \quad (18)$$

The diagonal elements are the ‘normal’ propagators. The off-diagonal elements are Gor’kov’s F and \bar{F} , respectively.

The phonon and electron Green function could be expanded in a Fourier series

$$D_\lambda(\mathbf{q}, \tau) = \frac{1}{\beta} \sum_{n=-\infty}^{\infty} e^{-i\nu_n \tau} D_\lambda(\mathbf{q}, i\nu_n) \quad (19)$$

$$G(\mathbf{k}, \tau) = \frac{1}{\beta} \sum_{n=-\infty}^{\infty} e^{-i\omega_n \tau} G(\mathbf{k}, i\omega_n), \quad (20)$$

where where $\nu_n = 2n\pi/\beta$ and $\omega_n = (2n + 1)\pi/\beta$ with integer n are the Matsubara frequencies. They are odd multiples of π/β for Fermions while for Bosons they are even.

2.2 Migdal-Eliashberg theory

The basic components of a many-body system are the propagators and the Migdal-Eliashberg theory [8–14] is no exception. The one-electron Green function for the non-interacting system, in momentum space at imaginary frequencies, is given by

$$G_0(\mathbf{k}, i\omega_n) = [i\omega_n \mathbf{1} - \varepsilon_{\mathbf{k}} \sigma_3]^{-1} \quad (21)$$

and for the phonons

$$D_0(\mathbf{q}, i\nu_n) = [M (\omega^2(\mathbf{q}) + \nu_n^2)]^{-1}, \quad (22)$$

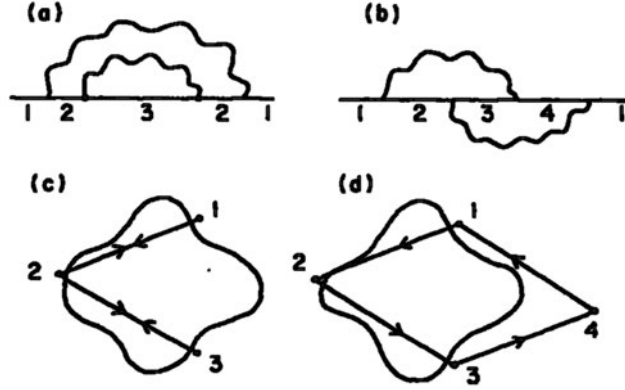


Fig. 1: Feynman diagrams (a) and (b) are the corrections of second order in the electron-phonon interaction to the electron propagator. Diagram (a) is included in Migdal theory while (b) is the first omitted diagram. Panels (c) and (d) shown schematic Fermi surfaces and particular k -states that contribute to (a) and (b), respectively. The last term, in general, will involve large energy denominators (as 3-4 and 1-4) such that it is negligible. This theorem may fail in two circumstances: (i) when either phonon has $|\mathbf{q}|$ small, or (ii) when the Fermi surface has a one-dimensional topology.

where M is the ion mass and $\omega(\mathbf{q})$ the phonon dispersion.

From a diagrammatic analysis a Dyson-like equation for the electron and phonon Green functions can be written, though now for the electron it will be a 2×2 matrix equation

$$[G(\mathbf{k}, i\omega_n)]^{-1} = [G_0(\mathbf{k}, i\omega_n)]^{-1} - \Sigma(\mathbf{k}, i\omega_n), \quad (23)$$

$$[D(\mathbf{q}, i\nu_n)]^{-1} = [D_0(\mathbf{q}, i\nu_n)]^{-1} - \Pi(\mathbf{q}, i\nu_n). \quad (24)$$

where Σ is the electronic and Π the phonon self-energy. In principle, in these self-energies, contain the full electron-phonon vertex. Migdal's theorem states that vertex corrections are small. It is therefore a good approximation to set the vertex to the bare vertex, meaning that the electron-phonon interaction is truncated at order $\sqrt{m/M} \sim \omega_D/E_F$. The self energy is then approximated as

$$\Sigma(\mathbf{k}, i\omega_n) = -\frac{1}{\beta} \sum_{\mathbf{k}'n'\nu} \sigma_3 G(\mathbf{k}', i\omega_{n'}) \sigma_3 \left[|g_{\mathbf{k},\mathbf{k}',\nu}|^2 D_\nu(\mathbf{k} - \mathbf{k}', i\omega_n - i\omega_{n'}) + V_C(\mathbf{k} - \mathbf{k}') \right], \quad (25)$$

where $V_C(\mathbf{k} - \mathbf{k}')$ is the screened Coulomb potential, cf. (13), which has been taken to depend only on the momentum transfer $\mathbf{k} - \mathbf{k}'$.

It is important to remember that $\hat{\Sigma}$ is a 2×2 matrix. It can be rewritten using the Pauli matrices

$$\Sigma(\mathbf{k}, i\omega_n) = i\omega_n [1 - Z(\mathbf{k}, i\omega_n)] \mathbb{1} + \chi(\mathbf{k}, i\omega_n) \sigma_3 + \phi(\mathbf{k}, i\omega_n) \sigma_1 + \bar{\phi}(\mathbf{k}, i\omega_n) \sigma_2. \quad (26)$$

We can now use the Dyson equation to replace the Green function matrix in the Migdal approximation to the self-energy (25). Solving the resulting system of equations for the components of the self-energy will give us the Eliashberg equations.

Using the notation of (26), the electronic Dyson becomes

$$[G(\mathbf{k}, i\omega_n)]^{-1} = i\omega_n Z \mathbb{1} - (\varepsilon_{\mathbf{k}} + \chi) \sigma_3 - \phi \sigma_1 - \bar{\phi} \sigma_2. \quad (27)$$

Inverting this 2×2 matrix, we obtain the Green matrix

$$\begin{aligned} G(\mathbf{k}, i\omega_n) &= \frac{1}{\Theta} \left[i\omega_n Z \mathbf{1} + (\varepsilon_{\mathbf{k}} + \chi) \sigma_3 + \phi \sigma_1 + \bar{\phi} \sigma_2 \right] \\ &= \frac{1}{\Theta} \begin{pmatrix} i\omega_n Z + (\varepsilon_{\mathbf{k}} + \chi) & \phi - i\bar{\phi} \\ \phi + i\bar{\phi} & i\omega_n Z - (\varepsilon_{\mathbf{k}} + \chi) \end{pmatrix}, \end{aligned} \quad (28)$$

with the determinant of (27)

$$\Theta = (i\omega_n Z)^2 - (\varepsilon_{\mathbf{k}} + \chi)^2 - \phi^2 - \bar{\phi}^2. \quad (29)$$

We see that the poles of the Green function matrix, i.e., the electron (and hole) elementary excitations, are given by $\det G(\mathbf{k}, \omega) = \Theta(\mathbf{k}, \omega) = 0$

$$E_{\mathbf{k}} = \sqrt{\left(\frac{\varepsilon_{\mathbf{k}} + \chi}{Z} \right)^2 + \frac{\phi^2 + \bar{\phi}^2}{Z^2}}, \quad (30)$$

thus the gap function is given by

$$\Delta(\mathbf{k}, i\omega_n) = \frac{\phi - i\bar{\phi}}{Z}. \quad (31)$$

Inserting (27) in the Migdal approximation to the self-energy (25), we obtain a system of nonlinear equations for the components of the self-energy. For $\phi = \bar{\phi} = 0$ the system is diagonal and a solution always exists. It corresponds to the normal state. In this case Z and χ are determined by the normal-state self-energy: χ shifts the electronic energies and Z is a renormalization function [8].

If an additional solution with non-zero ϕ or $\bar{\phi}$ exists, it has lower free energy and describes a superconducting state with gap function (31). Actually, it can be shown that, if in the Hamiltonian there are no terms describing spin-dependent interactions, ϕ and $\bar{\phi}$ satisfy identical nonlinear equations hence the solution will have $\phi = \bar{\phi}$, except for a proportionality factor.²

The explicit form of the system of equations for the components of the self-energy is

$$\begin{aligned} i\omega_n [1 - Z(\mathbf{k}, i\omega_n)] &= \frac{1}{\beta} \sum_{\mathbf{k}'n'\nu} |g_{\mathbf{k},\mathbf{k}',\nu}|^2 D_{\nu}(\mathbf{k} - \mathbf{k}', i\omega_n - i\omega_{n'}) \frac{i\omega_{n'} Z(\mathbf{k}', i\omega_{n'})}{\Theta(\mathbf{k}', i\omega_{n'})} \\ \chi(\mathbf{k}, i\omega_n) &= \frac{1}{\beta} \sum_{\mathbf{k}'n'\nu} |g_{\mathbf{k},\mathbf{k}',\nu}|^2 D_{\nu}(\mathbf{k} - \mathbf{k}', i\omega_n - i\omega_{n'}) \frac{\chi(\mathbf{k}', i\omega_{n'}) + \varepsilon'_{\mathbf{k}}}{\Theta(\mathbf{k}', i\omega_{n'})} \\ \phi(\mathbf{k}, i\omega_n) &= -\frac{1}{\beta} \sum_{\mathbf{k}'n'\nu} [|g_{\mathbf{k},\mathbf{k}',\nu}|^2 D_{\nu}(\mathbf{k} - \mathbf{k}', i\omega_n - i\omega_{n'}) - V_C(\mathbf{k} - \mathbf{k}')] \frac{\phi(\mathbf{k}', i\omega_{n'})}{\Theta(\mathbf{k}', i\omega_{n'})} \\ \bar{\phi}(\mathbf{k}, i\omega_n) &= -\frac{1}{\beta} \sum_{\mathbf{k}'n'\nu} [|g_{\mathbf{k},\mathbf{k}',\nu}|^2 D_{\nu}(\mathbf{k} - \mathbf{k}', i\omega_n - i\omega_{n'}) - V_C(\mathbf{k} - \mathbf{k}')] \frac{\bar{\phi}(\mathbf{k}', i\omega_{n'})}{\Theta(\mathbf{k}', i\omega_{n'})} \\ n &= 1 - \frac{2}{\beta} \sum_{\mathbf{k}'n'} \frac{\chi(\mathbf{k}', i\omega_{n'}) + \varepsilon_{\mathbf{k}'}}{\Theta(\mathbf{k}', i\omega_{n'})} \end{aligned}$$

²The arbitrary phase comes from the one of the one-electron state. Normally, the physical quantities cannot depend on this phase. However, it is measured by Josephson tunnelling. Thus BCS theory exhibits a broken gauge symmetry.

These are the *Eliashberg equations*. The last equation gives the electron density and determines the chemical potential μ .

The general Eliashberg equations couple all momenta \mathbf{k} . To simplify them, they are usually averaged over by replacing the sums over momenta by integrals over energy, weighted with the density of states. The result is a single set of equations. This approximation turns out to be good for elemental superconductors, but fails in describing more complex systems.

The \mathbf{k} -dependence in G comes mainly from the explicit $\varepsilon_{\mathbf{k}}$ dependence of Θ , while it can be averaged out in Z and ϕ (fixing $\varepsilon_{\mathbf{k}} = E_F$ because these quantities are non-zero only near the Fermi surface), so

$$\begin{aligned} Z(\mathbf{k}, i\omega_n) &\rightarrow \langle Z(\mathbf{k}, i\omega_n) \rangle_{\varepsilon=E_F} = Z(i\omega_n) \\ \phi(\mathbf{k}, i\omega_n) &\rightarrow \langle \phi(\mathbf{k}, i\omega_n) \rangle_{\varepsilon=E_F} = \phi(i\omega_n) \\ \chi(\mathbf{k}, i\omega_n) &\rightarrow \langle \chi(\mathbf{k}, i\omega_n) \rangle_{\varepsilon=E_F} = \chi(i\omega_n) \end{aligned}$$

On the right hand side of the Eliashberg equations the same \mathbf{k} average can be obtained by applying the operator $\frac{1}{N(0)} \sum_{\mathbf{k}} \delta(\varepsilon_{\mathbf{k}})$ where $N(0)$ is the normal density of states at the Fermi level and introducing a unity factor $\int d\omega \delta(\omega - \omega_{\mathbf{q},\nu})$, where $\mathbf{q} = \mathbf{k} - \mathbf{k}'$ is the phonon wavevector³

$$\begin{aligned} [1 - Z(i\omega_n)] i\omega_n &= -\frac{1}{\beta N^2(0)} \sum_{n'} \int d\omega \sum_{\mathbf{k}\mathbf{k}'\nu} \frac{|g_{\mathbf{k},\mathbf{k}',\nu}|^2 \delta(\varepsilon_{\mathbf{k}'}) \delta(\varepsilon_{\mathbf{k}}) \delta(\omega - \omega_{\mathbf{q},\nu}) 2\omega_{\mathbf{q},\nu}}{(\omega_n - \omega_{n'})^2 + \omega_{\mathbf{q},\nu}^2} \\ &\quad \times \int_{-\infty}^{\infty} d\varepsilon \frac{N(\varepsilon) i\omega_{n'} Z(i\omega_{n'})}{\Theta(\varepsilon, i\omega_{n'})} \\ \phi(i\omega_n) &= \frac{1}{\beta N^2(0)} \sum_{n'} \int d\omega \sum_{\mathbf{k}\mathbf{k}'\nu} \frac{|g_{\mathbf{k},\mathbf{k}',\nu}|^2 \delta(\varepsilon'_{\mathbf{k}}) \delta(\varepsilon_{\mathbf{k}}) \delta(\omega - \omega_{\mathbf{q},\nu}) 2\omega_{\mathbf{q},\nu}}{(\omega_n - \omega_{n'})^2 + \omega_{\mathbf{q},\nu}^2} \\ &\quad \times \int_{-\infty}^{\infty} d\varepsilon \frac{N(\varepsilon) \phi(i\omega_{n'})}{\Theta(\varepsilon, i\omega_{n'})} \\ \chi(i\omega_n) &= -\frac{1}{\beta N^2(0)} \sum_{n'} \int d\omega \sum_{\mathbf{k}\mathbf{k}'\nu} \frac{|g_{\mathbf{k},\mathbf{k}',\nu}|^2 \delta(\varepsilon'_{\mathbf{k}}) \delta(\varepsilon_{\mathbf{k}}) \delta(\omega - \omega_{\mathbf{q},\nu}) 2\omega_{\mathbf{q},\nu}}{(\omega_n - \omega_{n'})^2 + \omega_{\mathbf{q},\nu}^2} \\ &\quad \times \int_{-\infty}^{\infty} d\varepsilon \frac{N(\varepsilon) [\varepsilon + \chi(i\omega_{n'})]}{\Theta(\varepsilon, i\omega_{n'})} \\ n &= 1 - \frac{2}{\beta N(0)} \sum_{n'} \int_{-\infty}^{\infty} d\varepsilon \frac{N(\varepsilon) [\varepsilon + \chi(i\omega_{n'})]}{\Theta(\varepsilon, i\omega_{n'})}. \end{aligned}$$

as the phonon interaction is very low, the sum over \mathbf{k}' has been split up into an angular average for $\varepsilon_{\mathbf{k}} = E_F$ and an integration in ε on the ε dependence of the electronic Green function. Only the states near the Fermi level will contribute to this integral, because of the $\varepsilon_{\mathbf{k}}$ terms in $\Theta(\varepsilon, i\omega_n)$. When the density of states can be considered constant in this region, a further simplification can be introduced using $N(0)$ instead of $N(\varepsilon)$ and performing the integrals analytically. In this way the final result is $\chi(i\omega_n) = 0$ and $n = 1$ (half-filling approximation).

³The equation for χ will be omitted from now on because, in many cases, its contribution can be neglected.

It is useful to define the electron-boson spectral function, the positive-definite function

$$\begin{aligned}\alpha^2 F(\omega) &= N(0) \sum_{\mathbf{q}\nu} g_{\mathbf{q},\nu}^2 \delta(\omega - \omega_{\mathbf{q},\nu}) \\ &= \frac{1}{N(0)} \sum_{\mathbf{k}\mathbf{k}'} \sum_{\nu} |g_{\mathbf{k},\mathbf{k}',\nu}|^2 \delta(\varepsilon_{\mathbf{k}'}) \delta(\varepsilon_{\mathbf{k}}) \delta(\omega - \omega_{\mathbf{q},\nu}),\end{aligned}\quad (32)$$

where

$$g_{\mathbf{q},\nu}^2 = \frac{1}{N^2(0)} \sum_{\mathbf{k}'} |g_{\mathbf{k},\mathbf{k}',\nu}|^2 \delta(\varepsilon_{\mathbf{k}+\mathbf{q}}) \delta(\varepsilon_{\mathbf{k}}) \quad (33)$$

is the \mathbf{q} -dependent electron-phonon coupling. With this the Eliashberg system takes the form

$$\begin{aligned}[1 - Z(i\omega_n)] i\omega_n &= -\frac{\pi}{\beta} \sum_{n'} \frac{Z(i\omega_{n'}) i\omega_{n'}}{\Xi(i\omega_{n'})} \int d\Omega \frac{2\Omega \alpha^2 F(\Omega)}{(\omega_n - \omega_{n'})^2 + \Omega^2} \\ \phi(i\omega_n) &= \frac{\pi}{\beta} \sum_{n'} \frac{\phi(i\omega_{n'})}{\Xi(i\omega_{n'})} \left[\int d\Omega \frac{2\Omega \alpha^2 F(\Omega)}{(\omega_n - \omega_{n'})^2 + \Omega^2} - N(0) \bar{V}_C \right] \\ \Xi(i\omega_n) &= \sqrt{[Z(i\omega_n) \omega_n]^2 + [\phi(i\omega_n)]^2},\end{aligned}$$

where \bar{V}_C represents an appropriate Fermi surface average of the screened Coulomb potential V_C . The sum over Matsubara frequencies can be cut off at an energy ω_C . Solving these equations, we obtain the electron self-energy at the Fermi level.

2.3 Coulomb pseudopotential

Including the repulsive term in the Eliashberg equations is a hard task. The Coulomb interaction cannot be introduced with the same accuracy of the electron-phonon one, since it does not have a natural cut-off to ensure a convergent sum over the Matsubara frequencies. While the electron-electron interaction has a large energy scale and a correspondingly short interaction time, the electron-phonon interaction has a timescale typical of the much larger inverse phonon frequencies. The time scale difference is normally dealt using an energy window ω_C with a renormalized electron-electron interaction [13]

$$\mu^* = \frac{\mu}{1 + \mu \ln(E_F/\omega_C)}, \quad (34)$$

which is called *Morel-Anderson pseudopotential*. In this formula, μ is an average electron-electron matrix element times the density of states at the Fermi level.

In the normal state self-energy the Coulomb potential is already included, so that only the off-diagonal term will be affected by this correction, giving

$$\phi_C(i\omega_n) = -\mu^* \frac{\pi}{\beta} \sum_{n'} \frac{\phi(i\omega_{n'})}{\Xi(i\omega_{n'})} \theta(\omega_C - |\omega_{n'}|). \quad (35)$$

Including this contribution in the Eliashberg equation for ϕ , we obtain

$$\begin{aligned}\Delta(i\omega_n) Z(i\omega_n) &= \frac{\pi}{\beta} \sum_{n'} \frac{\Delta(i\omega_{n'})}{\sqrt{\omega_{n'}^2 + \Delta^2(i\omega_n)}} [\lambda(i\omega_{n'} - i\omega_n) - \mu^*(\omega_C)] \theta(\omega_C - |\omega_{n'}|) \\ Z(i\omega_n) &= 1 + \frac{\pi}{\omega_n \beta} \sum_{n'} \frac{\omega_{n'}}{\sqrt{\omega_{n'}^2 + \Delta^2(i\omega_n)}} \lambda(i\omega_{n'} - i\omega_n)\end{aligned}$$

where $\lambda(i\omega_{n'} - i\omega_n)$ is related to the electron-boson spectral density $\alpha^2 F(\omega)$ through the relation

$$\lambda(i\omega_{n'} - i\omega_n) = \int_0^\infty d\Omega \frac{2\Omega\alpha^2 F(\Omega)}{\Omega^2 + (\omega_{n'} - \omega_n)^2}. \quad (36)$$

3 Real-axis Eliashberg equations

The Green function can be analytically continued onto the real-frequencies axis, by using the expression $\omega + i\delta$, with an infinitesimal δ . The density of states is contained in the imaginary part of $G(\mathbf{k}, \omega + i\delta)$.

In their real-axis formulation, the Eliashberg equations are a set of two non-linear integral equations for a complex frequency-dependent gap $\Delta(\omega)$ and a renormalization function $Z(\omega)$, which exists also in the normal state. Both $\Delta(\omega)$ and $Z(\omega)$ are temperature dependent.

$$\begin{aligned} \Delta(\omega, T)Z(\omega, T) &= \int_0^{\omega_C} d\omega' \Re \left[\frac{\Delta(\omega', T)}{\sqrt{\omega'^2 - \Delta^2(\omega', T)}} \right] \int_0^\infty d\Omega \alpha^2 F(\Omega) \\ &\quad \times \left\{ [n(\Omega) + f(-\omega')] \left[\frac{1}{\omega + \omega' + \Omega + i\delta^+} - \frac{1}{\omega - \omega' - \Omega + i\delta^+} \right] \right. \\ &\quad \left. - [n(\Omega) + f(\omega')] \left[\frac{1}{\omega - \omega' + \Omega + i\delta^+} - \frac{1}{\omega + \omega' - \Omega + i\delta^+} \right] \right\} \\ &\quad - \mu^* \int_0^{\omega_C} d\omega' \Re \left[\frac{\Delta(\omega', T)}{\sqrt{\omega'^2 - \Delta^2(\omega', T)}} \right] [1 - 2f(\omega')] \\ [1 - Z(\omega, T)]\omega &= \int_0^\infty d\omega' \Re \left[\frac{\omega'}{\sqrt{\omega'^2 - \Delta^2(\omega', T)}} \right] \int_0^\infty d\Omega \alpha^2 F(\Omega) \\ &\quad \times \left\{ [n(\Omega) + f(-\omega')] \left[\frac{1}{\omega + \omega' + \Omega + i\delta^+} - \frac{1}{\omega - \omega' - \Omega + i\delta^+} \right] \right. \\ &\quad \left. - [n(\Omega) + f(\omega')] \left[\frac{1}{\omega - \omega' + \Omega + i\delta^+} - \frac{1}{\omega + \omega' - \Omega + i\delta^+} \right] \right\}. \end{aligned}$$

Here, ω_C is the boson energy cut-off introduced in the Coulomb pseudo potential and $f(\omega) = 1/(e^{\beta\omega} + 1)$ is the Fermi, $n(\Omega) = 1/(e^{\beta\Omega} - 1)$ the Bose function. The real part of the product $\Delta(\omega, T)Z(\omega, T)$ and of $Z(\omega, T)$ is determined by the principal-value integrals, while the imaginary part comes from the delta-function parts.

The denominators can vanish for particular energies. Then the integrals must be done carefully when a numerical approach is used. The low frequency behaviour of the various functions is, at $T = 0$, $\Re[\Delta(\omega)] = c$, $\Im[\Delta(\omega)] = 0$, $\Re[Z(\omega)] = d$ and $\Im[Z(\omega)] = 0$ while, at $T \neq 0$, $\Re[\Delta(\omega)] \propto \omega^2$, $\Im[\Delta(\omega)] \propto \omega$, $\Re[Z(\omega)] = d(T)$ and $\Im[Z(\omega)] \propto 1/\omega$ where c and d are constants.

4 Simplified approaches

4.1 BCS limit

In order to better understand the Eliashberg equations, it can be useful to reduce them to BCS limit. To achieve this aim further approximations are introduced: First of all, the bosons factor in the real-axis Eliashberg equations are ignored, i.e., real bosons scattering are not taken into account. Further, the imaginary parts of Δ and Z must be neglected. We set

$$\Delta(\omega, T) = \begin{cases} \Delta_0(T) & \text{for } \omega < \omega_D \\ 0 & \text{for } \omega \geq \omega_D \end{cases}, \quad (37)$$

where $\Delta_0(T)$ is a real number and ω_D is the Deybe energy and replace $Z(\omega, T)$ by its value in the normal state at $\omega = 0$ and $T = 0$. Then

$$Z(0, T) - 1 = 2 \int_0^\infty d\omega' \int_0^\infty d\Omega \alpha^2 F(\Omega) \left[\frac{f(-\omega')}{(\omega' + \Omega)^2} + \frac{f(\omega')}{(\omega' + \Omega)^2} \right] \equiv \lambda(T), \quad (38)$$

which in the $T \rightarrow 0$ limit is

$$Z(0, 0) - 1 = \int_0^\infty d\Omega \alpha^2 F(\Omega) \int_0^\infty \frac{2d\omega'}{(\omega' + \Omega)^2} \equiv \lambda. \quad (39)$$

The gap equation becomes

$$\Delta_0(T) = \int_{\Delta_0(T)}^{\omega_D} d\omega' \frac{\Delta_0(T)}{\sqrt{\omega'^2 - \Delta_0^2(T)}} \frac{\lambda - \mu^*}{1 + \lambda} \left[1 - 2f(\omega') \right]. \quad (40)$$

It is interesting to note that now ω_D is important for both the λ and the μ^* contribution.

With $\varepsilon = \sqrt{\omega'^2 - \Delta_0^2}$, the equation can be rewritten as

$$\Delta_0(T) = \frac{\lambda - \mu^*}{1 + \lambda} \int_0^{\omega_D} d\varepsilon \frac{\Delta_0(T)}{\sqrt{\varepsilon^2 + \Delta_0^2(T)}} \left[1 - 2f\left(\sqrt{\varepsilon^2 + \Delta_0^2(T)}\right) \right], \quad (41)$$

which is the usual BCS equation at finite temperature. In the the $T \rightarrow 0$ limit it becomes

$$\Delta_0 = \frac{\lambda - \mu^*}{1 + \lambda} \int_0^{\omega_C} d\varepsilon \frac{\Delta_0}{\sqrt{\varepsilon^2 + \Delta_0^2}}, \quad (42)$$

which corresponds to the BCS gap equation if we define $\lambda_{\text{BCS}} = (\lambda - \mu^*)/(1 + \lambda)$. The renormalization factor $1/(1 + \lambda)$ comes from the Z term in the Eliashberg equation, i.e., from having included electron-phonon effects.

4.2 Critical temperature

Solving the Eliashberg system, even in the isotropic form, is a quite demanding task. However the most relevant results can be obtained using a simpler approach proposed by McMillan [15]. Through a fit of a large set of results obtained using the spectral function of lead and solving the

Eliashberg equations in a small range of the parameter space ($\lambda < 2$ and $\mu^* < 0.15$), McMillan obtained an analytic formula for the critical temperature:

$$T_C = \frac{\Theta_D}{1.45} \exp \left[-\frac{1.04(1+\lambda)}{\lambda - \mu^*(1+0.62\lambda)} \right], \quad (43)$$

where Θ_D is the Debye temperature and the number λ has the same meaning as the electron-phonon coupling parameter, and can be derived from the Eliashberg function as

$$\lambda = 2 \int d\Omega \frac{\alpha^2 F(\Omega)}{\Omega}. \quad (44)$$

Later, this formula was refined by Allen and Dynes [15], who substituted the factor $\Theta_D/1.45$ with $\Omega_{log}/1.2$, with the much more representative frequency

$$\Omega_{log} = \exp \left[\frac{2}{\lambda} \int d\Omega \log \Omega \frac{\alpha^2 F(\Omega)}{\Omega} \right], \quad (45)$$

which is a weighted average of the phonon frequencies. The McMillan formula predicts an upper limit for T_C even if λ increases indefinitely. However this was a wrong conclusion because the equation (43) was not derived analytically but obtained by numerical solutions in a fixed range of the coupling constant and then it is not possible to consider the limit for $\lambda \rightarrow \infty$. For $\lambda \gg 1$, taking the limit of the Eliashberg equations the following expression for T_C can be obtained in an analytical way

$$T_C = 0.183\omega_D\sqrt{\lambda} \quad (46)$$

and it is clear that in Eliashberg theory there is no upper limit for the critical temperature.

In general the Eliashberg equations are solved numerically with an iterative method until you reach self-consistency. The numerical procedure is very simple in the formulation on imaginary axis, much less so on the real one. The critical temperature can be calculated or by solving an eigenvalue equation [8] or, more easily, by giving a very small test value to superconducting gap (for the Pb it is $\Delta = 1.4$ meV at $T = 0$ K so, for example, $\Delta(T) = 10^{-7}$ meV) and checking at which temperature the solution converges. In this way, T_c is obtained with accuracy superior to experimental error bars.

5 Relation between real- and imaginary-axis formulation

5.1 Padé method for analytic continuation

The Eliashberg equations on the real axis are very difficult to solve, while their formulation on the imaginary axis, while simpler to solve, can be used almost only to evaluate the critical temperature. Therefore, a procedure which allows obtaining the real-axis gap and the renormalization function by analytically continuing $\Delta(i\omega_n)$ and $Z(i\omega_n)$ is often used [16]. This procedure makes use of Padé approximants. It speed up the numerical solution of Eliashberg equations. However the Padé method is valid only at $T < T_C/10$, thus it is often necessary

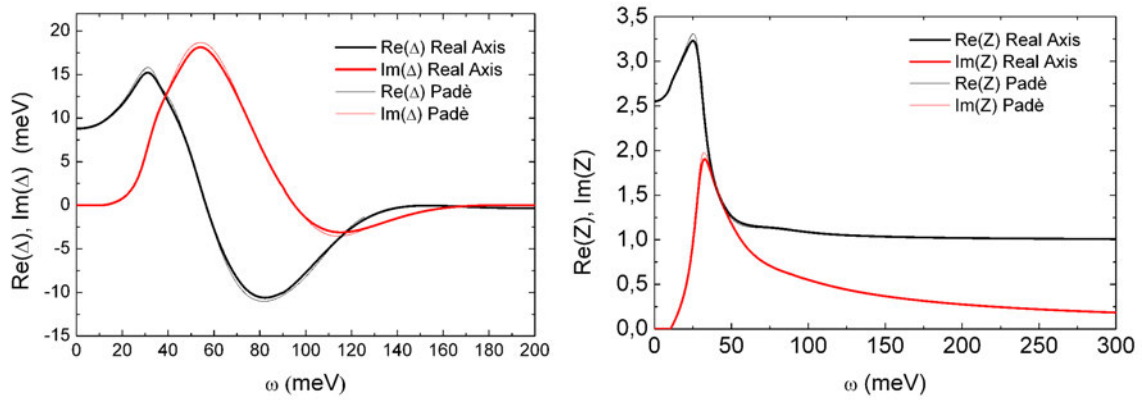


Fig. 2: Validity check of Padé approximants methods. Here real and imaginary part of $\Delta(\omega)$ and $Z(\omega)$ are shown at $T < T_C/10$.

to still solve for $\Delta(\omega)$ directly from the real-frequency equations. Also when the Eliashberg equations contain some terms that describe the presence of impurities in the superconductor the accuracy of the Padé approximants can leave something to be desired.

The N -point Padé approximant to a complex function $u(z)$ of the complex variable z , whose N values $u_i = u_i(z_i)$ ($i = 1, \dots, N$) are given at N complex points z_i , is defined as the continued fraction

$$C_N(z) = \frac{a_1}{1 + \frac{a_2(z - z_1)}{1 + \frac{a_3(z - z_2)}{1 + \frac{a_4(z - z_3)}{1 + \frac{\vdots}{1 + a_n(z - z_{n-1})}}}}} \quad (47)$$

such that

$$C_N(z_i) = u_i, \quad i = 1, \dots, N. \quad (48)$$

The coefficients a_i are given by recursive formula $a_i = g_i(z_i)$, where

$$g_1(z_i) = u_i \quad \text{with } i = 1, \dots, N$$

$$g_p(z) = \frac{g_{p-1}(z_{p-1}) - g_{p-1}(z)}{(z - z_{p-1})g_{p-1}(z)} \quad \text{for } p \geq 2$$

It can be shown that the continued fraction can be evaluated order-by-order via $C_N(z) = A_N(z)/B_N(z)$ where A_N and B_N are polynomials given by the recursion relation

$$A_{n+1}(z) = A_n(z) + (z - z_n)a_{n+1}A_{n-1}(z) \quad \text{with } n = 1, 2, \dots, N - 1$$

$$B_{n+1}(z) = B_n(z) + (z - z_n)a_{n+1}B_{n-1}(z) \quad \text{with } n = 1, 2, \dots, N - 1$$

with starting values $A_0 = 0$, $A_1 = a_1$, and $B_0 = B_1 = 1$.

A comparison of results obtained with the real-axis equations and results obtained with the Padé method is shown in Fig. 2.

5.2 Marsiglio, Schossmann, and Carbotte formulation

A more recent method [10] for solving the Eliashberg equations on the real axis introduces two equations for the renormalized frequency $\tilde{\omega}(z) = zZ(z)$ and the pairing function $\phi(z)$

$$\begin{aligned} \tilde{\omega}(\omega) &= \omega + i\pi T \sum_{m=1}^{\infty} \frac{\tilde{\omega}(i\omega_m)}{\sqrt{\tilde{\omega}^2(i\omega_m) + \phi^2(i\omega_m)}} [\lambda(\omega - i\omega_m) - \lambda(\omega + i\omega_m)] \\ &+ i\pi \int_{-\infty}^{\infty} dz \frac{\tilde{\omega}(\omega - z)}{\sqrt{\tilde{\omega}^2(\omega - z) - \phi^2(\omega - z)}} \alpha^2 F(z) [n(z) + f(z - \omega)] \end{aligned} \quad (49)$$

$$\begin{aligned} \phi(\omega) &= i\pi T \sum_{m=1}^{\infty} \frac{\phi(i\omega_m)}{\sqrt{\tilde{\omega}^2(i\omega_m) + \phi^2(i\omega_m)}} [\lambda(\omega - i\omega_m) - \lambda(\omega + i\omega_m) - 2\mu^* \theta(\omega_C - |\omega_m|)] \\ &+ i\pi \int_{-\infty}^{\infty} dz \frac{\phi(\omega - z)}{\sqrt{\tilde{\omega}^2(\omega - z) - \phi^2(\omega - z)}} \alpha^2 F(z) [n(z) + f(z - \omega)]. \end{aligned} \quad (50)$$

These equations give solutions for the real-axis gap and renormalization function that are identical to those obtained from the solution of the real-axis equations. Then they are valid at any temperature, but their numerical solution presents problems completely analogous to those of the formulation on the real axis. The choice between these equations and those on the real axis is thus just a matter of personal taste.

6 Tunneling inversion of the standard Eliashberg equations

In the past $\alpha^2 F(\Omega)$ and μ^* were obtained by experimental data or were considered as free parameters. As shown in the lecture of R. Heid, now they can actually be calculated by density functional theory [17] so, the theory does not contain free parameters.

When such calculations are not possible, the standard method to obtain these physical input parameters involves single-particle tunneling spectroscopy, which is perhaps the simplest, most direct probe of the excitations of a solid. In these experiments electrons are injected into (or extracted from) a sample, as a function of bias voltage V . The typical example is a planar junction SIN (superconductor, thin layer of insulating and a metal in the normal state) [18]. The resulting current is proportional to the superconducting density of states [19]

$$I_S(V) \propto \int d\omega \Re \left[\frac{|\omega|}{\sqrt{\omega^2 - \Delta^2(\omega)}} \right] [f(\omega) - f(\omega + V)], \quad (51)$$

where we have used the gap function, $\Delta(\omega)$, defined as $\Delta(\omega) \equiv \phi(\omega)/Z(\omega)$. The proportionality constant contains information about the density of states of the normal metal and the tunneling matrix element. They are usually assumed to be constant.

In the zero temperature limit the derivative of the current with respect to the voltage is simply proportional to the superconducting density of states

$$\left(\frac{dI}{dV} \right)_S / \left(\frac{dI}{dV} \right)_N \propto \Re \left\{ \frac{|V|}{\sqrt{V^2 - \Delta^2(V)}} \right\}, \quad (52)$$

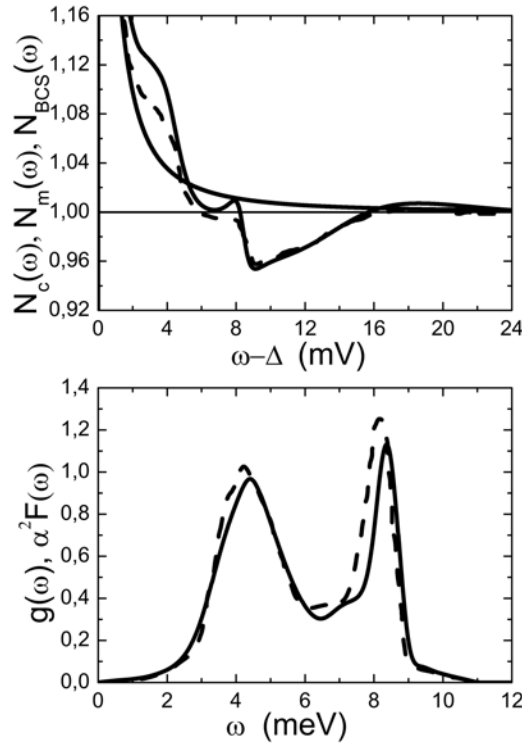


Fig. 3: Upper panel: Energy dependence of the lead density of states in the superconducting states at very low temperature ($T \ll T_c$). The dashed line represents experimental data obtained from tunneling, while BCS weak-coupling theory yields the dash-dotted line. The Eliashberg strong coupling result is shown by a solid line. Lower panel: Calculated electron phonon spectral function of Pb (solid line) determined by inversion of Eliashberg equations compared with the measured phonon density of states (dashed line) for the same material.

where S and N denote superconducting and normal state, respectively. The right hand side is simply the density of states, computed within the Eliashberg framework. From the experimentally measured quasiparticle density of states at very low temperature $N_m(V) = (\frac{dI}{dV})_S / (\frac{dI}{dV})_N$, where the subscript m denotes "measured", it is possible, through a complicated mathematical procedure, to obtain the electron-phonon spectral function $\alpha^2 F(\omega)$ and the Coulomb pseudopotential μ^* , not only for superconductors but also for normal metals via the proximity effect [19].

The procedure followed is conceptually simple but mathematically involved [20, 21]. A first guess is made for the two quantities, namely $\alpha^2 F_0(\omega)$, i.e., starting with a generic function greater than zero in a finite range and with a Coulomb pseudopotential parameter, $\mu_0^* \simeq 0.1$. So the Eliashberg equations (at $T = 0$) can be solved numerically with these two input parameters in order to obtain the complex function $\Delta(\omega)$ necessary for calculating the superconductive density of states $N_c^0(\omega)$ denoted by the subscript c (calculated) and 0 (for a first choice). Next, the functional derivative $\frac{\delta N_c^0(\omega)}{\delta \alpha^2 F(\nu)}$ which give the infinitesimal response of $N_c^0(\omega)$ to the change in $\alpha^2 F(\nu)$ is computed. This is used to make a second guess for $\alpha^2 F(\nu)$ through the equation $\delta \alpha^2 F_0(\nu) = \int d\omega [\frac{\delta N_c^0(\omega)}{\delta \alpha^2 F(\nu)}]^{-1} [N_m(\omega) - N_c^0(\omega)]$. The new electron phonon spectral function is

$\alpha^2 F_1(\nu) = \alpha^2 F_0(\nu) + \delta\alpha^2 F_0(\nu)$. This procedure is continued until convergence is reached. Unique $\alpha^2 F(\nu)$ and μ^* result. They are referred to as the measured microscopic parameters for that particular material. It is not at all apparent that the structures of the density of states, as can be seen in the upper panel of Fig. 3, reflect the shape of the electron-phonon spectral function, through the function $\Delta(\omega)$.

At zero temperature the gap function $\Delta(\omega)$ is real and roughly constant up to a certain energy equal to that constant. This implies that the density of states will have a gap, as in BCS theory. At finite temperature the gap function has a small imaginary part starting from zero frequency (and, in fact the real part approaches zero at zero frequency so that in principle there is no gap, even for an s-wave order parameter. In practice, a very well-defined gap still occurs for moderate coupling, and disappears at finite temperature only when the coupling strength is increased significantly.

McMillan and Rowell were able to deconvolve their measurement, to produce the single electron density of states. Since the superconducting density of states is given by the right hand side of (52), the structure in the data must reflect the structures in the gap function, $\Delta(\omega)$, that originate from the input function, $\alpha^2 F(\omega)$. In other words, the dI/dV curve can be viewed as as a highly nonlinear transform of $\alpha^2 F(\omega)$. Thus the, usually very small, structure present in the density of states contains important information (in coded form) concerning the electron-phonon interaction as can be seen in the lower panel of Fig. 3, where the calculated electron phonon spectral function of Pb determined by inversion of the Eliashberg equations is compared with the neutron scattering measurements of the phonon density of states for the same material: this is the most clear way to determine the mechanism of superconductivity in a material.

Once $\alpha^2 F(\omega)$ (and μ^*) has been acquired in this way one can use the Eliashberg equations to calculate other properties, for example, T_c or many others physical quantities (temperature dependence of the gap, of the upper critical field, of the specific heat etc). These can then be compared to experiment, and the agreement in general tends to be fairly good.

One may suspect, however, a circular argumentation, since the theory was used to produce the spectrum (from experiment), and now the theory is used as a predictive tool, with the same spectrum. There are a number of reasons, however, for believing that this procedure has produced meaningful information. First of all, the spectrum obtained comes out to be positive definite, as is physically required. Second, the spectrum is non-zero precisely in the phonon region, as it should be and it agrees very well with the measured spectrum. Moreover, as already mentioned, various thermodynamic properties are calculated with this spectrum, with good agreement with experiments. Finally, the density of states itself can be calculated in a frequency regime beyond the phonon region. The agreement with experiment is spectacular.

None of these indicators of success can be taken as definitive proof of the electron-phonon interaction. For example, even the excellent agreement with the density of states could be understood as a mathematical property of analytic functions. This procedure has not been so straightforward or possible in all superconductors.

An alternate inversion procedure, which utilizes a Kramers-Kronig relation to extract $\Delta(\omega)$ from the tunneling result and remove μ^* from the procedure has been provided [22]. At last a

procedure exists for obtaining the electron-phonon spectral density by inversion of optical conductivity data, a process very similar in spirit to the McMillan-Rowell inversion of tunnelling data. This procedure has the advantage that it can be utilized also in the normal state [23].

7 Approximations of the standard Eliashberg equations

As mentioned before, the standard Eliashberg theory has been formulated within a lot of approximations. Here a list of these simplifications with possible generalizations:

- **validity of Migdal's theorem:** In almost all superconductors the condition $\omega_D/E_F \ll 1$ is fulfilled. In HTCS and fullerenes $\omega_D/E_F \sim 10^{-1}$ and it is necessary to include vertex corrections in the self-energy [24].
- **single conduction band:** Before the discovery of MgB₂ the known superconductors could be described within one-band models. Then the theory has been generalized to two (MgB₂) [25] or more bands (iron pnictides).
- **isotropic order parameter:** In the oldest superconductors the order parameter does not depend on the position on the Fermi surface, i.e., $\Delta \equiv \Delta(\mathbf{k})$. There is experimental evidence that this is not true in HTCS [26–28].
- **singlet superconductivity:** Usually the spin of Cooper pairs is equal to zero, but in Sr₂RuO₄ [29] probably it equals one, implying a different spatial symmetry (*p*-wave) [8].
- **infinite conduction bandwidth:** In almost all superconductors the width of the conduction band is much larger than the representative energy of the boson mediating the Cooper pairs interaction (phonons, antiferromagnetic spin fluctuations) so that it can be considered to be infinite. In HTCS and Fullerenes this approximation breaks down and the real bandwidth has to be included in the theory [13].
- **half filling:** Typically the occupation of the conduction band is symmetric. In HTCS this is not true and the number of the Eliashberg equation increases because of $\chi(\omega) \neq 0$ [13].
- **flat normal density of states:** Generally the normal density of states can be approximated by a constant around the Fermi level. In PuCoGa₅ and in a small number of other compounds this approximation is not valid [30]. Also in this case the number of Eliashberg equations increases [8].
- **no disorder or magnetic impurities:** A material can be disordered with chemical doping or neutron irradiation, moreover magnetic impurities can be added. To describe these physical situations, new terms have to be introduced in the Eliashberg equations [31].
- **no proximity effect:** A thin layer of a noble metal on top of a superconductor can be described by means of a generalization of Eliashberg equations [14].

8 Cuprate high-temperature superconductors

The standard Eliashberg equations have been derived for superconductors where the energy gap showed an s -wave symmetry and the Cooper pairing was mediated by the electron-phonon interaction. This type of interaction allows the application of Migdal's theorem, which states that vertex corrections in the electron-phonon interaction can be neglected to order $\lambda\omega_D/E_F$. On the other hand, it is now widely accepted that the high T_c cuprates have an energy gap with d symmetry [26]. As concerns the microscopic mechanism leading to Cooper pairs, in these materials, there is still no consensus, even though there are indications that antiferromagnetic spin fluctuations can play an important role [28, 29]. In principle, different mechanisms can provide a transition to the superconducting state without any phonon participation. But a scenario where superconductivity occurs through a joint contribution of the phonon and electronic mechanisms is also perfectly realistic. If different mechanisms are considered the Migdal's theorem does not work a priori. In this case the vertex corrections, at least in principle, cannot be neglected and a new type of Eliashberg equations could be necessary. The simplest model of cuprates uses a single-band approximation in a two-dimensional case, thus referring, for example, to the a - b planes of the layered superconductors and neglecting the band dispersion and the gap in the c -direction. For simplicity, one can consider the Fermi surface as circle in the a - b plane and the wave vectors \mathbf{k} and \mathbf{k}' completely determined by the respective azimuthal angles ϕ and ϕ' , since their length is, as usual, taken equal to k_F . The d -wave one-band Eliashberg equations in the imaginary axis representation are [32]

$$\omega_n Z(i\omega_n, \phi) = \omega_n + \frac{T}{2} \sum_m \int_0^{2\pi} d\phi' \Lambda(i\omega_n - i\omega_m, \phi, \phi') N_Z(i\omega_m, \phi') + \Gamma \frac{N_Z(i\omega_n)}{c^2 + N_Z(i\omega_n)^2}$$

$$Z(i\omega_n, \phi) \Delta(i\omega_n, \phi) = \frac{T}{2} \sum_m \int_0^{2\pi} d\phi' [\Lambda(i\omega_n - i\omega_m, \phi, \phi') - \mu^*(\phi, \phi', \omega_c) \vartheta(\omega_c - \omega_m)] N_\Delta(i\omega_m, \phi')$$

where ϑ is the Heaviside function, ω_c a cut-off energy,

$$\Lambda(i\omega_n - i\omega_m, \phi, \phi') = 2 \int_0^{+\infty} d\Omega \alpha^2 F(\Omega, \phi, \phi') / [(\omega_n - \omega_m)^2 + \Omega^2],$$

$$N_\Delta(i\omega_m, \phi) = \frac{\Delta(i\omega_m, \phi)}{\sqrt{\omega_m^2 + \Delta^2(i\omega_m, \phi)}},$$

$$N_Z(i\omega_m, \phi) = \frac{\omega_m}{\sqrt{\omega_m^2 + \Delta^2(i\omega_m, \phi)}},$$

and

$$N_Z(i\omega_n) = \frac{1}{2\pi} \int_0^{2\pi} N_Z(i\omega_n, \phi) d\phi.$$

Γ is proportional to the impurity concentration or disorder and c is related to the electron phase shift for scattering off an impurity. The Born limit is found when $c = \infty$ but Γ/c^2 constant, and the unitary limit when $c = 0$. In the Born limit there is a different behavior between s - and d -symmetries: in the s -wave symmetry a non magnetic impurities do not affect the critical

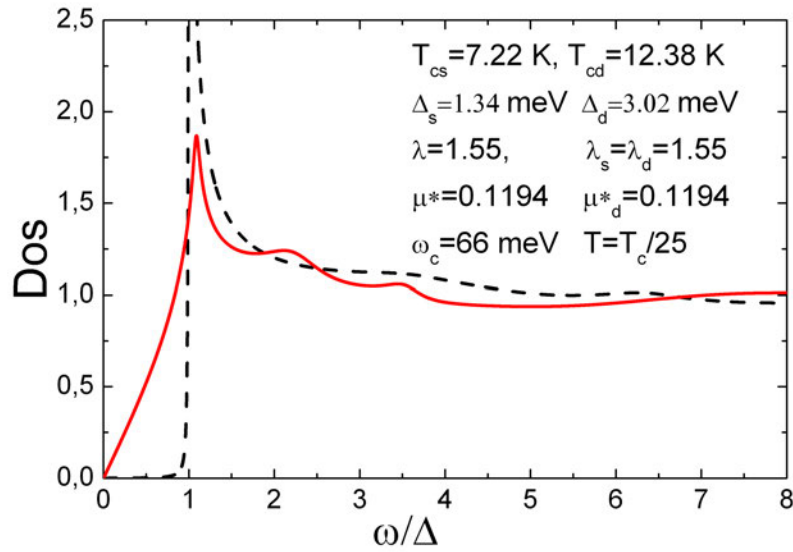


Fig. 4: The calculated superconductive density of states in the d -wave (red solid line) and s -wave (black dashed line) case.

temperature while in the d -wave symmetry the critical temperature is strongly reduced. In the simplest model the electron-boson spectral function $\alpha^2(\Omega)F(\Omega, \phi, \phi')$ and the Coulomb pseudopotential $\mu^*(\phi, \phi')$ to lowest order contain both s - and d -wave contributions,

$$\alpha^2 F(\Omega, \phi, \phi') = \alpha^2 F_s(\Omega) + \alpha^2 F_d(\Omega) \sqrt{2} \cos(2\phi) \sqrt{2} \cos(2\phi') \quad (53)$$

$$\mu^*(\phi, \phi') = \mu_s^* + \mu_d^*(\Omega) \sqrt{2} \cos(2\phi) \sqrt{2} \cos(2\phi'). \quad (54)$$

A solution with a pure d -wave gap function $\Delta(\omega, \phi') = \Delta_d(\omega) \cos(2\phi)$ and a pure s -wave renormalization function $Z(\omega, \phi') = Z_s(\omega)$ can be obtained. Indeed the equation for $Z_d(\omega)$ is a homogeneous integral equation whose only solution in the weak-coupling regime is $Z_d(\omega) = 0$. Even though in the strong-coupling limit a non-zero solution could exist above a certain coupling strength threshold, but usually one does not consider this rather exotic case and then the stable solution corresponds to $Z_d(\omega) = 0$ for all the couplings.

By assuming d -wave symmetry for the gap function, the parameter μ_s^* does not enter into the two relevant Eliashberg equations. Therefore, although it is certainly larger than μ_d^* and so drives the system towards d -wave symmetry, it does not influence the solution.

The superconductive density of states $N_d(\omega)$ can be easily obtained from the calculated frequency-dependent gap function as

$$N_d(\omega) = \int_0^{2\pi} \frac{d\phi}{2\pi} \Re \left\{ \frac{\omega}{\sqrt{\omega^2 - \Delta_d^2(\omega) \cos^2(2\phi)}} \right\}. \quad (55)$$

In Fig. 4 the superconductive density of states calculated in s - and d -wave cases are compared. The black-dotted line is the solution obtained for lead, the red-solid line is an ideal solution where the input parameters are kept the same of the case of lead, but d -wave symmetry has been imposed.

9 Multi-band Eliashberg theory

The equations seen so far (in all their formulations) are suitable to describe only a relatively small number of superconductors. There are many materials which are less trivial and show a multi-band structure. Consider a superconductor containing several different groups of electrons occupying distinct quantum states. The most typical example is a material with several overlapping energy bands. One can expect that each band will possess its own energy gap. This means that the density of states of the superconducting pairs contains several peaks. Of course if the energy gap were defined as the smallest quantum of energy that can be absorbed by the material, then only the smallest gap of the system would satisfy this definition. Thus to avoid misunderstandings when talking about the multi-gap structure of a spectrum we will mean explicitly the aforementioned multi-peak property of the density of states. For this case the previous equations must be generalized.

Considering a two band system [25] as the MgB₂, the parameters multiply: there are now four separate electron-phonon spectral functions $\alpha_{ij}^2 F(\Omega)$ and four Coulomb pseudopotentials μ_{ij}^* , where $i, j = 1, 2$.

The isotropic Eliashberg equations generalized to n bands ($i = 1, \dots, n$), are written on the imaginary axis as

$$\begin{aligned} \omega_n Z_i(i\omega_n) &= \omega_n + \pi T \sum_{mj} \lambda_{ij}(i\omega_n, i\omega_m) N_j^Z(i\omega_m) + \\ &+ \sum_j [\Gamma_{ij} + \Gamma_{ij}^M] N_j^Z(i\omega_n) \end{aligned} \quad (56)$$

$$\begin{aligned} Z_i(i\omega_n) \Delta_i(i\omega_n) &= \pi T \sum_{mj} [\lambda_{ij}(i\omega_n, i\omega_m) - \mu_{ij}^*(\omega_c)] \times \\ &\times \Theta(\omega_c - |\omega_m|) N_j^\Delta(i\omega_m) + \sum_j [\Gamma_{ij} + \Gamma_{ij}^M] N_j^\Delta(i\omega_n) \end{aligned} \quad (57)$$

where Γ_{ij} and Γ_{ij}^M are the non magnetic and magnetic impurity scattering rates, and, in a manner quite similar to the single band case,

$$\lambda_{ij}(i\omega_m - i\omega_n) \equiv 2 \int_0^\infty d\Omega \frac{\Omega \alpha_{ij}^2 F(\Omega)}{\Omega^2 + (\omega_n - \omega_m)^2} \quad (58)$$

and

$$N_j^\Delta(i\omega_m) = \Delta_j(i\omega_m) \cdot \left[\sqrt{\omega_m^2 + \Delta_j^2(i\omega_m)} \right]^{-1}, \quad N_j^Z(i\omega_m) = \omega_m \cdot \left[\sqrt{\omega_m^2 + \Delta_j^2(i\omega_m)} \right]^{-1}.$$

The diagonal elements describe the intra-band coupling, while the off-diagonal the inter-band one. The values of the inter-band coupling constants are not completely free, but there is a constraint

$$\frac{\lambda_{ij}}{\lambda_{ji}} = \frac{N_i(0)}{N_j(0)}. \quad (59)$$

This means that the ratio of the interband coupling constant λ_{12} and λ_{21} is equal to the ratio of density of states.

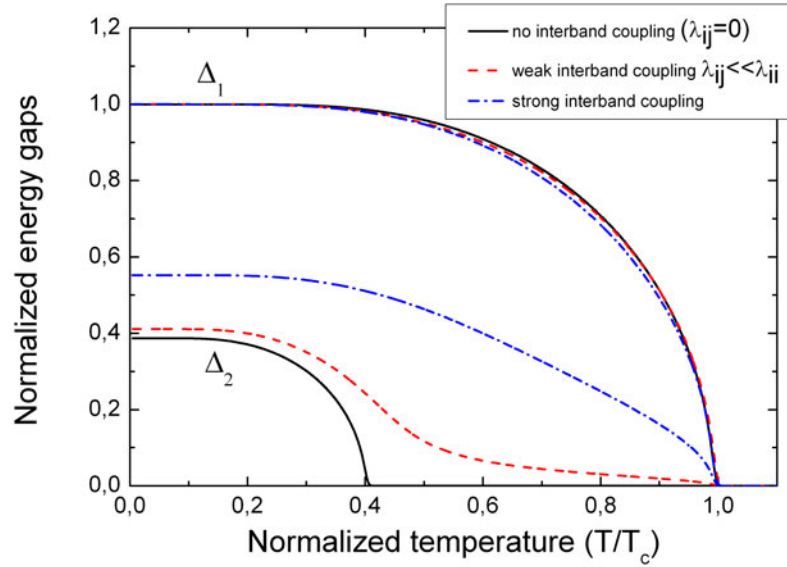


Fig. 5: Temperature dependence of the gaps Δ_1 and Δ_2 in a two-band model, calculated in the cases of (i) no intraband coupling (solid lines), (ii) weak intraband coupling (dotted lines), and (iii) strong interband coupling (dash-dot lines). The intraband coupling constants are arbitrary; here we used those for MgB_2

It is interesting and propedeutic for the subsequent chapters to analyze different situations, as the coupling constants change: the limit of small inter-band coupling and the opposite case, i.e., a pure inter-band case [25] will be considered. The first case is interesting because it allows understanding that an, even small, interband coupling leads to the correlation of the two bands, otherwise completely independent as it is shown Fig. 5.

In a superconductor without interband coupling ($\lambda_{ij} = \lambda_{ji} = 0$) the bands behaves as n different superconductors that have n different transition temperatures, T_{C1} and T_{C2} , each associated with the respective band. The resulting superconducting state that results will be given by the sum of the n bands contributions which are completely independent. As the off-diagonal components grow the n bands become connected. However, this does not means that the superconductor behaves as a one-band system. As long as each band has different a spectral function, and a different coupling constant, they will give different contributions. Changing the off-diagonal elements λ_{ij} results in different temperature of the upper and lower gaps. Each band contains its own set of Cooper pairs. Since, generally speaking, k_{F_i} and k_{F_j} (here k_{F_i} and k_{F_j} are on the Fermi surface for different bands), there is no pairing of electrons belonging to different energy bands i.e. λ_{ij} , of course, does not represent a pairing between electrons of different bands. This does not mean, however, that the pairing within each band is completely insensitive to the presence of the other. On the contrary, a peculiar interband interaction and the appearance of nonlocal coupling constants are fundamental properties of the multiband model. Consider two electrons belonging to band i . They exchange phonons and form a pair as a result. There exist two pairing scenarios. In one of them, the first electron emits a virtual phonon and makes a transition into a state within the same energy band. The second electron absorbs the phonon

and also remains in the same energy band, forming a bound pair with the first one. This is the usual pairing picture, described by a coupling constant λ_{ii} . However, the presence of the other energy band gives rise to an additional channel. Namely, the first electron, originally located in band i , can emit a virtual phonon and make a transition into band k . The phonon is absorbed by the second electron, which also is scattered into band k , where it pairs up with the first electron. As we know, there is no energy conservation requirement for single virtual transitions; such conservation, however, must hold for the initial and final states. In our case this criterion is met. Indeed, the initial and final states correspond to particles on the Fermi surface. Note that, in addition, the initial and final total momenta are equal to zero. Thus the initial state had two electrons in band i , while the final state finds a pair in band k . Interband charge transfer processes are described by nondiagonal coupling constants λ_{ij} , and because of them the system is characterized by a single critical temperature. Otherwise, each band would have its own T_c . There is a formal similarity between the Eliashberg equations for a proximity system [14] and those for a two band system: if the mathematical expression of Eliashberg theory for a system with two gaps is compared with a proximity system it is possible to notice a profound formal analogy between these two situations. In both cases there is induced superconductivity because in the second band, as in a noble metal film, a very weak intrinsic pairing can be chosen so this band alone would not become superconducting. However the mechanisms giving rise to induced superconductivity are very different. In the two band model the systems are “separated” in momentum space and the second band acquires an order parameter thanks to phonon exchange. The phase space for phonons is effectively increased. In the proximity effect, on the other hand, the systems are spatially separated and superconductivity is induced by the tunnelling of Cooper pairs.

The multiband Eliashberg model developed above can also be used to explain the temperature dependence of the upper critical magnetic field [33]. For the sake of completeness, the linearized gap equations in the presence of magnetic field, for a superconductor in the clean limit are reported. In the following, v_{F_j} is the Fermi velocity of the j -th band, and H_{c2} is the upper critical field

$$\begin{aligned}\omega_n Z_i(i\omega_n) &= \omega_n + \pi T \sum_{mj} \lambda_{ij}(i\omega_n - i\omega_m) \text{sign}(\omega_m) \\ Z_i(i\omega_n) \Delta_i(i\omega_n) &= \pi T \sum_{mj} [\lambda_{ij}(i\omega_n - i\omega_m) - \mu_{ij}^*(\omega_c)] \times \\ &\quad \times \theta(|\omega_c| - \omega_m) \chi_j(i\omega_m) Z_j(i\omega_m) \Delta_j(i\omega_m) \\ \chi_j(i\omega_m) &= \frac{2}{\sqrt{\beta_j}} \int_0^{+\infty} dq \exp(-q^2) \times \\ &\quad \times \tan^{-1} \left[\frac{q \sqrt{\beta_j}}{|\omega_m Z_j(i\omega_m)| + i \mu_B H_{c2} \text{sign}(\omega_m)} \right].\end{aligned}$$

Here $\beta_j = \pi H_{c2} v_{F_j}^2 / (2\Phi_0)$ and Φ_0 is the unit of magnetic flux. In these equations the bare Fermi velocities v_{F_j} [33] are the input parameters.

10 Iron pnictide superconductors

10.1 Gaps, critical temperature, and upper critical magnetic field

The new class of superconductive Fe-based compounds [34, 35] shows similar characteristics to the cuprates and the heavy fermions, for example the high values of the ratio $2\Delta/T_c$ or the presence of the pseudogap. For all three classes of materials it is proposed that superconductivity is mediated by antiferromagnetic spin fluctuations [28]. The most obvious difference is that almost all the iron compounds present a multiband behavior while in HTCS and in heavy fermions this behavior was detected only in some particular cases. The multi-band nature of Fe-based superconductors may give rise to a multi-gap scenario [36] that is indeed emerging from different experimental data with evidence for rather high gap ratios, $\approx 2 - 3$. In this regard neither a three-band BCS model is adequate (it can only account for the gap ratio and T_c but not for the exact experimental gap values) nor a four-band Eliashberg model with small values of the coupling constants and large boson energies because the calculated critical temperature has turned out to be larger than the experimental one. The high experimental value of the larger gap suggests that high values of the coupling constants might be necessary to explain the experimental data within a three-band model [37]: one has therefore to employ the Eliashberg theory for strong coupling superconductors. At the beginning a three-band Eliashberg model allowed reproducing various experimental data, indicating that these compounds can represent a case of dominant negative interband-channel superconductivity ($s\pm$ wave symmetry) with small typical boson energies (≈ 10 meV) but too high values of the electron-boson coupling constants ($1.9 \leq \lambda_{\text{tot}} \leq 5.9$). The way to solve this problem is suggested by experiments of Inosov and coworkers [38]: they found that the temperature evolution of the spin resonance energy follows the superconducting energy gap and this fact should indicate a *feedback effect* [28, 39, 40] of the condensate on the spin fluctuations.

Then the experimental low temperature spin resonance can be chosen as the representative boson energy and the two remaining free parameters can be fixed in order to reproduce the exact experimental gap values. After this, with the same parameters, the critical temperature T_c^* can be calculated. Generally it is always $T_c^* \gg T_c^{\text{exp}}$ where T_c^{exp} is the experimental critical temperature. In the next step the same temperature dependence of the superconductive gap has to be imposed to the representative boson energy while the other input parameters used before are kept fixed.

Of course, at $T = T_c^*$ the energy peaks of the spectral functions (the representative boson energy) is equal to zero while at $T = 0$ K the new spectral functions are equal to the old ones. In this way, by taking into account the *feedback effect* of the condensate [28, 39, 40] on the antiferromagnetic spin fluctuations it is possible to explain the experimental data (the gap values and the critical temperature) in a model with only two free parameters in a moderate strong coupling regime ($\lambda_{\text{tot}} \approx 1.5 - 2$).

Four representative cases are reported (three hole type and one electron type): $\text{LaFeAsO}_{1-x}\text{F}_x$, $\text{SmFeAsO}_{1-x}\text{F}_x$, $\text{Ba}_{1-x}\text{K}_x\text{Fe}_2\text{As}_2$, and $\text{Ba}(\text{Fe}_x\text{Co}_{1-x})_2\text{As}_2$. The electronic structure of the hole

type compounds can be approximately described by a three-band model with two hole bands (indicated in the following as bands 1 and 2) and one equivalent electron band (3) [37] while for one electron type compound the model contains one hole band (indicated in the following as band 1) and two equivalent electron bands (2 and 3) [41]. The s -wave order parameters of the hole bands Δ_1 and Δ_2 have opposite sign with respect to that of the electron band Δ_3 [42] in the hole type case while Δ_1 has opposite sign with respect to that of the two electron bands, Δ_2 and Δ_3 in the electron type case [41]. In such systems, in the first approximation, intraband coupling could only be provided by phonons ph , and interband coupling only by antiferromagnetic spin fluctuations sf [37, 39]. The experimental data concerning the four compounds considered can be summarized as follow [39]:

1. LaFeAsO_{0.9}F_{0.1} (LaFeAsOF) with $T_c^A = 28.6$ K where point-contact spectroscopy measurements gave $\Delta_1(0) \approx 8.0$ meV and $\Delta_2(0) \approx 2.8$ meV;
2. Ba_{0.6}K_{0.4}Fe₂As₂ (BaKFeAs) with $T_c = 37$ K where ARPES measurements gave $\Delta_1(0) = 12.1 \pm 1.5$ meV, $\Delta_2(0) = 5.2 \pm 1.0$ meV and $\Delta_3(0) = 12.8 \pm 1.4$ meV
3. SmFeAsO_{0.8}F_{0.2} (SmFeAsOF) with $T_c^A = 52$ K ($T_c^{\text{bulk}} = 53$ K) where point-contact spectroscopy measurements gave $\Delta_1(0) = 18 \pm 3$ meV and $\Delta_2(0) = 6.15 \pm 0.45$ meV;
4. Ba(Fe _{x} Co_{1- x})₂As₂ (BaFeCoAs) with $T_c^A = 22.6$ K ($T_c^{\text{bulk}} = 24.5$ K) where point-contact spectroscopy measurements gave $\Delta_1(0) = 4.1 \pm 0.4$ meV and $\Delta_2(0) = 9.2 \pm 1$ meV.

T_c^A is the critical temperature obtained by Andreev reflection measurements [36] and T_c^{bulk} is the critical temperature obtained by transport measurements. Note that only in the case of ARPES the gaps are associated to the relevant band since point-contact spectroscopy measurements generally gives only two gaps, the larger one has been arbitrarily indicated as Δ_1 supposing that $\Delta_1 \sim |\Delta_3|$. To obtain the gap-values and the critical temperature within the $s \pm$ wave, one has to solve six coupled equations for the gaps $\Delta_i(i\omega_n)$ and the renormalization functions $Z_i(i\omega_n)$, where i is the index of the bands and ranges from 1 to 3. The solution of the system of multiband Eliashberg equations requires a huge number of input parameters (18 functions and 9 constants); however, some of these parameters are related to one another, some can be extracted from experiments and some can be fixed by suitable approximations. In the case of the pnictides several assumptions can be made: (i) the total electron-phonon coupling constant is small, (ii) phonons mainly provide intraband coupling [42], (iii) spin fluctuations mainly provide interband coupling [42]. The simplest way to take these assumptions into account is to set $\lambda_{ii}^{ph} = \lambda_{ij}^{ph} = \lambda_{ii}^{sf} = 0$. Indeed the upper limit of the phonon coupling in these compounds is ≈ 0.35 [43], and the intraband spin-fluctuation coupling can be neglected [42]. Moreover, the phonon couplings and the Coulomb pseudopotentials roughly compensate each other, then $\mu_{ii}^*(\omega_c) = \mu_{ij}^*(\omega_c) = 0$ [37]. Within these approximations, the electron-boson coupling-constant matrix λ_{ij} becomes [37, 39, 41]:

$$\lambda_{ij} = \begin{pmatrix} 0 & \lambda_{12} & \lambda_{13} \\ \lambda_{21} = \lambda_{12}\nu_{12} & 0 & \lambda_{23} \\ \lambda_{31} = \lambda_{13}\nu_{13} & \lambda_{32} = \lambda_{23}\nu_{23} & 0 \end{pmatrix} \quad (60)$$

	λ_{tot}	$\lambda_{\text{tot}}^{\text{old}}$	$\lambda_{12/21}$	$\lambda_{13/31}$	$\lambda_{23/32}$	Ω_0 (meV)
BaFeCoAs	1.87		0.76/0.85	1.21/5.44	0.00/0.00	9.04
	2.83	1.93	0.91/1.02	2.08/9.35	0.00/0.00	9.04
	1.72		0.77/0.87	1.05/4.72	0.00/0.00	9.04
	2.52		0.90/1.01	1.76/7.91	0.00/0.00	9.04
	1.75		0.00/0.00	2.11/1.91	0.40/0.21	11.44
LaFeAsOF	2.38	2.53	0.00/0.00	2.93/2.66	0.46/0.24	11.44
	2.04		0.00/0.00	2.27/2.27	0.56/0.28	14.80
BaKFeAs	2.84	3.87	0.00/0.00	3.21/3.21	0.67/0.34	14.80
	1.72		0.00/0.00	1.55/3.88	0.42/0.84	20.80
SmFeAsOF	2.39	5.90	0.00/0.00	2.23/5.58	0.49/0.98	20.80

Table 2: The values of Ω_0 and λ_{ij} , that allow reproducing the experimental gap values, are shown. λ_{tot} is compared with $\lambda_{\text{tot}}^{\text{old}}$ that is the value determined in the previous works [37, 41]. In the first rows the *sf* spectral functions used have usual shape while in the second ones have Lorentzian shape.

where $\nu_{ij} = N_i(0)/N_j(0)$ and $N_i(0)$ is the normal density of states at the Fermi level for the *i*-th band. In the hole case $\lambda_{21} = \lambda_{12} = 0$ while in the electron case $\lambda_{23} = \lambda_{32} = 0$.

In the numerical simulations the standard form for the antiferromagnetic spin fluctuations is used: $\alpha_{ij}^2 F^{sf}(\Omega) = B_{ij} \Omega \Omega_{ij} \Theta(\Omega_{\text{max}} - \Omega) / (\Omega^2 + \Omega_{ij}^2)$ where B_{ij} are the normalization constants necessary to obtain the proper values of λ_{ij} while Ω_{ij} are the peak energies. In all the calculations, for simplicity, $\Omega_{ij} = \Omega_0$. The maximum spin-fluctuation energy is $\Omega_{\text{max}} = 10\Omega_0$, the cut-off energy is $\omega_c = 30\Omega_0$ and the maximum quasiparticle energy is $\omega_{\text{max}} = 40\Omega_0$. The typical *sf* energy Ω_0 is the spin resonance energy that has been measured and the empirical relation $\Omega_0 = (2/5)T_c$ available in literature [44] is assumed to be correct for all compounds examined.

Bandstructure calculations provide information about the factors ν_{ij} that enter the definition of λ_{ij} . In the case of $\text{LaFeAsO}_{0.9}\text{F}_{0.1}$, $\nu_{13} = 0.91$ and $\nu_{23} = 0.53$; for $\text{Ba}_{0.6}\text{K}_{0.4}\text{Fe}_2\text{As}_2$, $\nu_{13} = 1$ and $\nu_{23} = 2$; in $\text{SmFeAsO}_{0.8}\text{F}_{0.2}$, $\nu_{13} = 0.4$ and $\nu_{23} = 0.5$ and in $\text{Ba}(\text{Fe}_x\text{Co}_{1-x})_2\text{As}_2$, $\nu_{12} = 1.12$ and $\nu_{13} = 4.50$ [39].

First of all the imaginary-axis Eliashberg equations are solved in order to calculate the low-temperature values of the gaps (which are actually obtained by analytical continuation to the real axis by using the technique of the Padé approximants) and so the two free parameters

	$\Delta_1(\text{meV})$	$\Delta_2(\text{meV})$	$\Delta_3(\text{meV})$	$T_c(\text{K})$	$T_c^*(\text{K})$
BaFeCoAs	6.63	-4.07	-9.18	26.07	33.00
	7.02	-4.12	-9.18	23.73	28.95
	5.89	-3.78	-8.17	23.43	29.69
	6.19	-3.79	-8.19	21.72	26.41
LaFeAsOF	8.01	2.82	-7.75	29.37	37.22
	8.01	2.77	-7.71	26.86	31.81
BaKFeAs	12.04	5.20	-12.00	43.66	55.26
	12.04	5.24	-11.91	38.33	46.18
SmFeAsOF	14.86	6.15	-18.11	58.53	74.13
	15.51	6.15	-18.00	52.80	63.82

Table 3: The calculated values of the gaps and of the two critical temperature with and without feedback effect. In the first rows the *sf* (spin-fluctuation) spectral functions used have the usual shape while in the second line they have Lorentzian shape.

of the model are fixed: λ_{13} and λ_{23} (λ_{12}). By properly selecting the values of λ_{13} and λ_{23} (λ_{12}) it is relatively easy to obtain the experimental values of the gaps with reasonable values of $\lambda_{tot} = \sum_{ij} N_i(0)\lambda_{ij} / \sum_{ij} N_i(0)$ (between 1.72 and 2.04). However, in all the materials examined, the high $2\Delta_{1,3}/k_B T_c$ ratio (of the order of 8-9) makes it possible to reproduce *also* the values of the large gap(s) only if the calculated critical temperature T_c^* is considerably higher than the experimental one. For solving this problem, that is also present in the HTCS, it is necessary to assume the existence a feedback effect [28, 39] of the condensate and, in a phenomenological way, a temperature dependence of the representative boson energy $\Omega_0(T) = \Omega_0 \tanh(1.76\sqrt{T_c^*/T} - 1)$ that is, approximately, the temperature dependence of the gap in the strong coupling case, is introduced in the Eliashberg equation.

The primary effect of this assumption is the reduction of the critical temperature without changes in the gap values at $T \ll T_c^*$. For a completely consistent procedure it should be used $\Omega_0(T) = \Omega_0 \eta(T)$ where $\eta(T)$ is the temperature dependent part of the superfluid density $\rho(T) = \rho(0)\eta(T)$ and $\rho(0)$ is the superfluid density at $T = 0$ K. $\eta(T)$ is a function of $\Delta_i(i\omega_n)$ and so, in this way, the numerical solution of the Eliashberg equations becomes remarkably more complex and time consuming.

For a general picture of the physical landscape the Eliashberg equations have to be solved in three different situations: (i) only *sf* inter-band coupling is present and the *sf* spectral functions

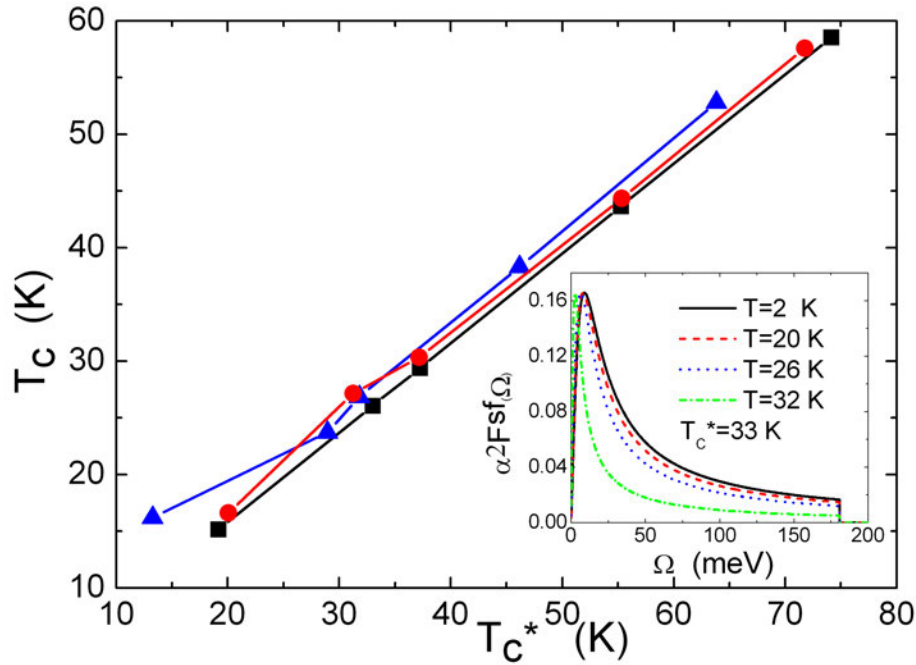


Fig. 6: Calculated critical temperature T_c with feedback effect versus standard critical temperature T_c^* in three different situations: only interband sf coupling with standard spectral functions (black squares), interband sf coupling with standard spectral functions and small intraband ph coupling (red circles) and only interband sf coupling with Lorentz spectral functions (dark blue triangles). The insert shows the sf spectral function, for $Ba(Fe_xCo_{1-x})_2As_2$ at different temperatures ($T < T_c^*$) with the feedback effect.

have the usual shape of the normal state (ii) sf interband coupling with a small ph intra-band contribution is present and sf spectral functions have the usual shape, and (iii) only sf interband coupling is present and the sf spectral functions have Lorentz shape.

In the first case the coupling constant λ_{tot} is in the range 1.72-2.04. The results are almost independent from Ω_{max} . The agreement with the experimental critical temperature is good. It is important to notice that the coupling parameters almost do not change in these considered case. In the second case there is also an intra-band phonon contribution, equal in each band and in each compound for simplicity, with $\lambda_{ii}^{ph} = 0.35$ and $\Omega_0^{ph} = 18$ meV that are the upper limits for the ph coupling constants and the representative ph energies [43]. The ph spectral functions have Lorentzian shape [37]. The phonon peaks are all in $\Omega_{ij} = \Omega_0^{ph}$, and the antiferromagnetic spin fluctuations peak in $\Omega_{ij} = \Omega_0^{sf}$ and the half-width⁴ is always 2 meV [39] and $\omega_c = 12\Omega_0^{ph}$. λ_{tot} and T_c are practically the same as the previous case. This last fact indicates that the effect of intraband phonon contributions is negligible. In the third case (Lorentz shape of sf spectral functions) the agreement with the experimental critical temperatures is very good in all compounds but the total coupling is larger ($2.38 \leq \lambda_{\text{tot}} \leq 2.84$).

⁴In more recent work the half-width of the Lorentzian functions describing antiferromagnetic spin fluctuations is equal to $\Omega_0^{sf}/2$ [38].

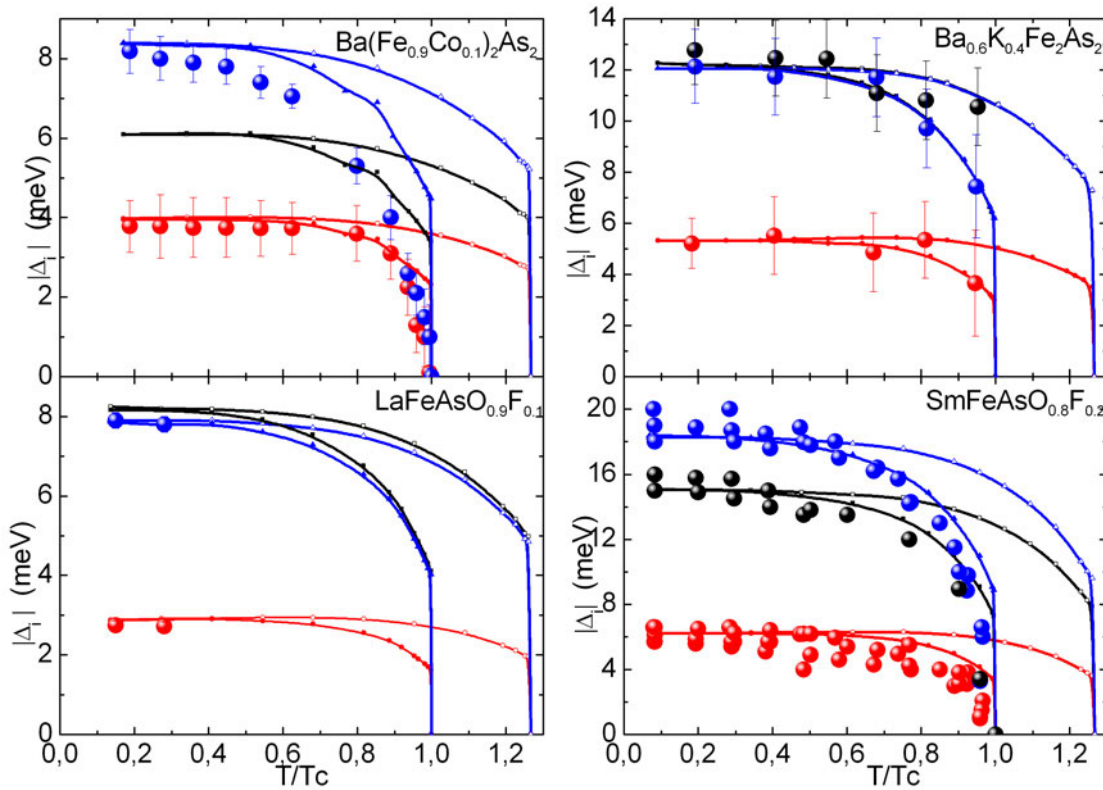


Fig. 7: Calculated temperature dependence of $|\Delta_i|$ from the solution of real axis Eliashberg equations in the standard case (open symbol) and when the feedback effects are present (solid symbol): $|\Delta_1|$ black, $|\Delta_2|$ red, and $|\Delta_3|$ dark blue. The experimental data [39] are shown as big solid bullets.

Fig. 6 shows the linear relation between T_c and T_c^* in all three cases examined. In Table 2 the input parameters of the Eliashberg equations in the first and third case examined for the four compounds are listed. Table 3 summarizes the calculated values of the gaps and critical temperatures T_c and T_c^* obtained by numerical solution of the Eliashberg equations. Once the values of the low-temperature gaps were obtained, the temperature dependence can be calculated by directly solving the three-band Eliashberg equations in the real-axis formulation instead of using the analytical continuation to the real axis of the imaginary-axis solution. Of course, the results of the two procedures are virtually identical at low temperature.

In Fig. 7 the calculated temperature dependence of $|\Delta_i|$ is compared with the experimental data and the agreement is very good. In all cases, their behavior is rather unusual and completely different from the BCS since the gaps slightly decrease with increasing temperature until they suddenly drop close to T_c . This arises from a complex non-linear dependence of the Δ vs. T curves on the λ_{ij} values and is possible only in a strong-coupling regime [45]. Curiously, in all four compounds the rate T_c^*/T_c is the same, 1.27. The three-band Eliashberg equations for the upper critical field [40] are solved. Here the three bare Fermi velocities v_{Fj} are the input parameters. The number of adjustable parameters can be reduced to one by assuming that, as in

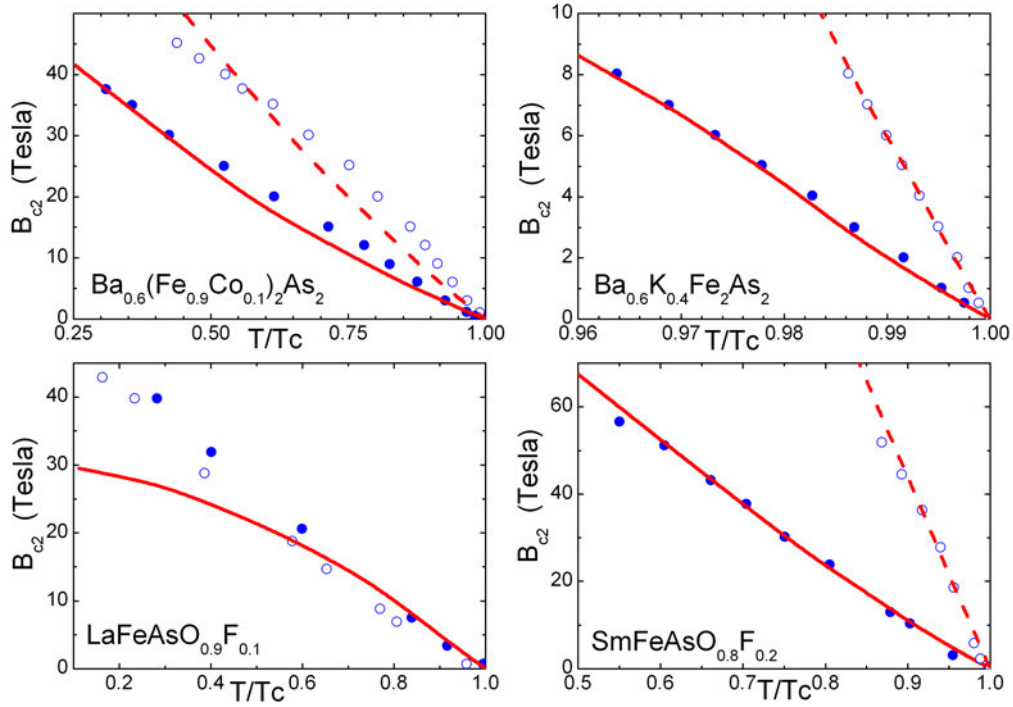


Fig. 8: Experimental temperature dependence of the upper critical field in $Ba(Fe_xCo_{1-x})_2As_2$, $LaFeAsO_{0.9}F_{0.1}$, $Ba_{0.6}K_{0.4}Fe_2As_2$, and $SmFeAsO_{0.8}F_{0.2}$ (symbols), and the relevant fitting curves (lines) obtained by solving the Eliashberg equations. $H \parallel ab$: Solid symbols, solid line and $H \parallel c$: open symbols, dashed line.

a free-electron gas, $v_{F_j} \propto N_j(0)$ so that $v_{F_2} = v_{F_1}\nu_2/\nu_1$ and $v_{F_3} = v_{F_1}/\nu_1$, thus leaving v_{F_1} as the only free parameter.

Fig. 8 depicts the experimental values of the upper critical field measured [40] in the case of $Ba(Fe_xCo_{1-x})_2As_2$, $Ba_{0.6}K_{0.4}Fe_2As_2$, $LaFeAsO_{0.9}F_{0.1}$, and $SmFeAsO_{0.8}F_{0.2}$ compared to the best-fitting curve obtained by solving the Eliashberg equations as discussed above. The quality of the fit is rather good in almost all cases, which is a remarkable result of the model in spite of the crudeness of the free-electron approximation. The phenomenology of iron-pnictides superconductors can be explained in the framework of a three-band $s\pm$ wave Eliashberg theory with only two free parameters plus a *feedback effect* i.e., the effect of the condensate on the antiferromagnetic spin fluctuations responsible of the superconductivity in these compounds. Indeed in the four iron compounds discussed, it is possible to reproduce the experimental critical temperature, the gap values and the upper critical field in a moderate strong-coupling regime: $\lambda_{tot} \approx 1.7 - 2.0$. The large value of the ratio between the gaps and the critical temperature finds a natural justification in this model. Eventually, for describing the phenomenology of the iron compound $LiFeAs$, it is necessary to use $s\pm$ four-band Eliashberg equations in a moderate strong coupling regime $\lambda_{tot} = 1.6$ and also in this case the agreement with the experimental data is good [46].

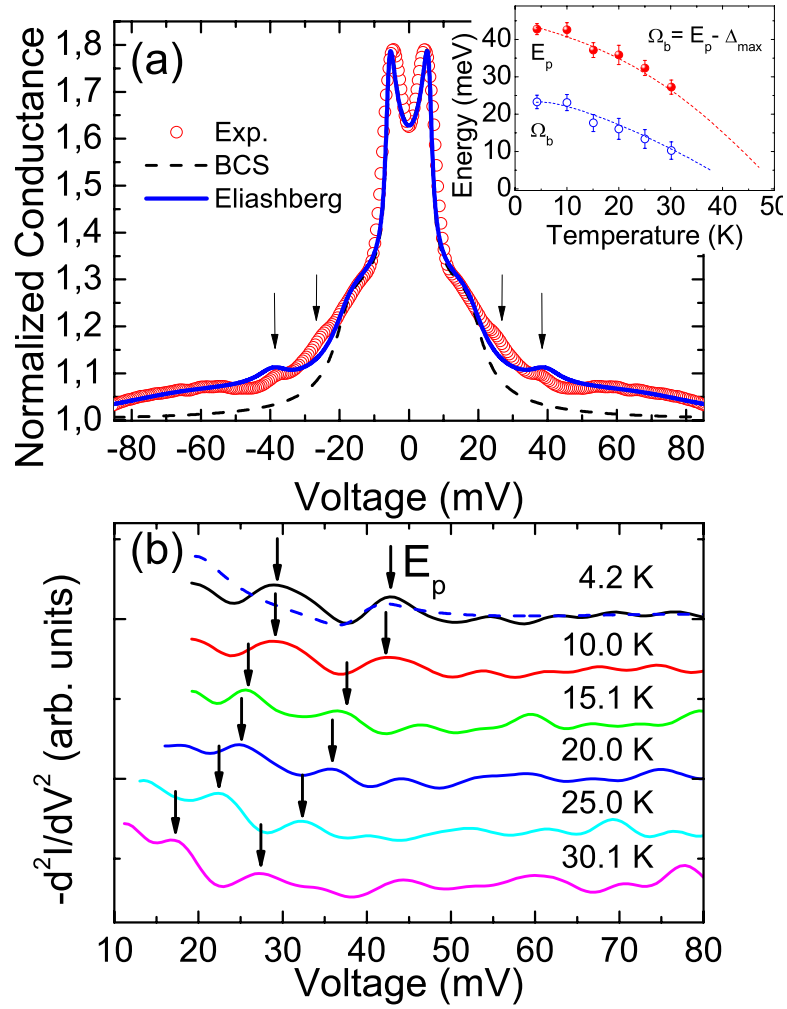


Fig. 9: (a) Normalized experimental conductance curve (circles) obtained in a $\text{Ag}/\text{SmFeAsO}_{0.8}\text{F}_{0.2}$ point-contact. The dashed line is a BTK fit to the experiment, obtained using the constant BCS values for the gaps. The solid line is a theoretical curve obtained by introducing in the BTK model the energy-dependent gap functions calculated within the three-band Eliashberg theory. (b) Temperature dependence of the $-d^2I/dV^2$ curves obtained from the same contact as in (a), showing the displacement of the bosonic structures with increasing temperature. The dashed line is obtained from the theoretical curve shown in (a). Inset: temperature dependence of the energy peak, E_p (full symbols) extracted from (b) together with the corresponding boson energy $\Omega_b(T) = E_p(T) - \Delta_{max}(T)$. Lines are guides to the eye.

10.2 Interaction mechanism

In moderate- or strong-coupling superconductors the tunneling or the Andreev reflection [36] conductance curves can show signatures of the energy dependence of the superconducting gap. These structures are more easily observable if the amplitude of the Andreev signal is large; their signature in the second derivative of the I - V curve can be related to the electron-boson spectral function. In the following, results obtained in an iron compound that provide examples of such strong-coupling effects and of their analysis will be shown, they strongly support a

spin-fluctuation-mediated origin of superconductivity if compared with the inelastic neutron scattering measurements.

Fig. 9 shows a normalized experimental conductance curve obtained on an optimally doped $\text{SmFeAsO}_{0.8}\text{F}_{0.2}$ polycrystal (circles). The amplitude of the Andreev signal in this contact is exceptionally high [36] (about 80%) and, in addition to the clear two-gap features (peaks and shoulders), additional structures or small kinks can be seen around 27 and 40 meV. The dashed line is a BTK [36] fit to the experiment using the two-band 2D BTK model with BCS gap values (i.e. independent of energy). The fit reproduces very well the experiment in the central part of the curve (and allows obtaining reliable values of the gaps) but fails at higher energies. The solid line is instead the result of inserting in the same BTK model the energy-dependent order parameters obtained by solving the three-band Eliashberg equations in which, as usual, the electron-boson spectral function is modeled by a Lorentzian curve [36]. Since to the best of the present knowledge no spin-resonance energy value is available for this compound, the characteristic energy has been chosen, following [44], by extrapolating the relationship $\Omega_0 = 2T_c/5 \approx 20$ meV. Although the theoretical curve shows no structure at 27 meV, the feature at 40 meV is remarkably well reproduced as can be observed in Fig. 9 (a) and (b) (dashed line). Only the structure present at approximately $\Omega_0 + \Delta_{max}$ is reproduced and this indicates that the model has to be investigated further or that additional features of the spectral function are playing an important role. As expected, both structures shift in energy on increasing temperature, partly because the amplitude of the superconducting gaps is also decreasing.

The inset to Fig. 9 (a) reports the position of the energy peak in the second derivative, E_p (full symbols) and the values of the characteristic energy of the boson spectrum $\Omega_b = E_p - \Delta_{max}$ (open symbols) as a function that decreases in temperature. This means that Ω_b cannot be the energy of a phonon mode (in that case it would not tend to zero!) and thus rules out a phononic origin of this feature. Instead, the trend of Ω_b is very similar to that of the spin-resonance energy peak reported in the paper of Inosov *et al.* [38] and thus strongly supports a spin-fluctuation mediated pairing mechanism in these compounds.

This three bands Eliashberg model has only two free parameter λ_{13} and λ_{23} and it is able to explain the values of the gaps, the structures after the gaps in the point-contact spectra the critical temperature, the dependence of temperature of the upper critical field etc. Similar results can be obtained [41] for $\text{Ba}(\text{Fe}_x\text{Co}_{1-x})_2\text{As}_2$.

11 Conclusion

The theory of Eliashberg is, in principle, a theory without free parameters, because the two input parameters, the electron-phonon spectral function and the Coulomb pseudopotential can be calculated via the Density Functional Theory (DFT). From the solution of the Eliashberg equations on the real axis all the physical observables can then be calculated through, almost always, simple functions of complex quantities $\Delta(\omega, T)$ and $Z(\omega, T)$ that, of course, have to be calculated numerically. Obviously, in the majority of cases, the materials of interest can not be described by a *s*-wave model. However, using the appropriate generalizations, the phenomenol-

ogy of almost all superconductors (except HTCS underdoped for now) can be reproduced by this formalism. This theory, strictly speaking, is neither a theory from first principles nor a purely phenomenological theory, and this is both its strength – it has a very close relationship with the experimental observation – and its weakness – no one has ever discovered a new superconductor based on the Eliashberg theory.⁵ To be sure, no one has ever discovered a new superconductor reasoning on any theory.

Acknowledgment

I thank Sara Galasso for valuable help.

⁵The main reason is that the energies involved are too small and the accuracy required cannot be achieved in the calculations.

References

- [1] J. Bardeen, L.N. Cooper, J.R. Schrieffer, *Phys. Rev. B* **108**, 1175 (1957)
- [2] L. Pitaevskii: *Phenomenology and Microscopic Theory: Theoretical Foundations* in K.H. Bennemann and John B. Ketterson (eds.): *Superconductivity* (Springer, 2008)
- [3] W. Jones and N.H. March, *Theoretical Solid State Physics* (Dover Publications, 1973)
- [4] A.B. Migdal, *Sov. Phys. JETP* **34**, 996 (1958)
- [5] G.M. Eliashberg, *Sov. Phys. JETP* **11**, 696 (1960); *Sov. Phys. JETP* **12**, 1000 (1961)
- [6] Y. Nambu, *Phys. Rev.* **117**, 648 (1960)
- [7] V. Ambegaokar: *The Green's functions method* in R.D. Parks (ed.): *Superconductivity*, Vol. I (Dekker, New York, 1969)
- [8] P.B. Allen and B. Mitrović: *Theory of Superconducting T_c* in *Solid State Physics*, Vol. **37**, (1983)
- [9] D.J. Scalapino: *The Electron-phonon interaction and strong-coupling superconductor* in R.D. Parks (ed.): *Superconductivity*, Vol. I (Dekker, New York, 1969)
- [10] J.P. Carbotte, *Rev. Mod. Phys. B* **62**, 1027 (1990)
- [11] J.P. Carbotte and F. Marsiglio: *Electron-Phonon Superconductivity* in K.H. Bennemann and John B. Ketterson (eds.): *Superconductivity* (Springer, 2008)
- [12] E.R. Margine and F. Giustino, *Phys. Rev. B* **87**, 024505 (2013)
- [13] F. Marsiglio, *J. Low Temp. Phys.* **87**, 659 (1992)
- [14] V.Z. Kresin, H. Morawitz, S.A. Wolf: *Mechanisms of Conventional and High T_c Superconductivity* (Oxford University Press, 1993)
- [15] P.B. Allen and R.C. Dynes, *Phys. Rev. B* **12**, 905 (1975)
- [16] H.J. Vidberg and J.W. Serene, *J. Low Temp. Phys.* **29**, 179 (1977);
C.R. Leavens and D.S. Ritchie, *Solid State Communication*, **53**, 137, (1985)
- [17] D.S. Sholl, J.A. Steckel: *Density Functional Theory* (Wiley, 2009);
E. Engel, R.M. Dreizler: *Density Functional Theory* (Springer, Heidelberg, 2011)
- [18] I. Giaever and K. Megerle, *Phys. Rev. Lett.* **122**, 1101 (1961)
- [19] E.L. Wolf, *Principles of electron tunneling spectroscopy* (Oxford University Press, 1985)

- [20] W.L. Mc Millan and J.M. Rowell, Phys. Rev. Lett. **14**, 108 (1965);
Phys. Rev. Lett. **178**, 897 (1968)
- [21] W.L. Mc Millan and J.M. Rowell, *Tunneling and strong-coupling superconductivity*
in R.D. Parks (ed.): *Superconductivity*, Vol. I (Dekker, New York, 1969)
- [22] A.A. Galkin, A.I. D'yachenko, V.M. Svistunov, Sov. Phys.-JETP **39**, 1115 (1974)
- [23] F. Marsiglio, T. Startseva and J.P. Carbotte, Phys. Lett. A **245**, 172 (1998)
- [24] L. Pietronero, S. Strässler and C. Grimaldi, Phys. Rev. B **52**, 10516 (1995);
C. Grimaldi, L. Pietronero and S. Strässler, Phys. Rev. B **52**, 10530 (1995)
- [25] E.J. Nicol and J.P. Carbotte, Phys. Rev. B **71**, 054501 (2005)
- [26] E. Schachinger and J.P. Carbotte:
Extended Eliashberg theory for d-wave superconductivity and application to cuprate
in J.K. Sadasiva and S.M. Rao (eds.): *Models and Methods of High-Tc Superconductivity*,
Vol. II (Nova Science Publisher, 2003)
- [27] M.L. Kubic, Physics Reports **338**, 1 (2000); E.G. Maksimov, M.L. Kubic, and O.V. Dolgov,
Advances in Condensed Matter Physics **2010**, 423725 (2010)
- [28] A.V. Chubukov, D. Pines, and J. Schmalian:
A Spin Fluctuation Model for d-Wave Superconductivity
in K.H. Bennemann and John B. Ketterson (eds.): *Superconductivity* (Springer, 2008)
- [29] D. Manske, I. Eremin, and K.H. Bennemann:
Electronic Theory for Superconductivity in High-Tc Cuprates and Sr₂RuO₄
in K.H. Bennemann and John B. Ketterson (eds.): *Superconductivity* (Springer, 2008)
- [30] F. Jutier, G.A. Ummarino, J.C. Griveau, F. Wastin, E. Colineau, J. Rebizant, N. Magnani
and R. Caciuffo, Phys. Rev. B **77**, 024521 (2008)
- [31] A.A. Golubov, I.I. Mazin, Phys. Rev. B **55**, 15146 (1997)
- [32] G.A. Ummarino, R. Caciuffo, H. Chudo, S. Kambe Phys. Rev. B **82**, 104510 (2010);
D. Daghero, M. Tortello, G.A. Ummarino, J.-C. Griveau, E. Colineau, A.B. Shick, R.
Caciuffo, J. Kolorenc and A.I. Lichtenstein, Nature Communications **3**, 786, (2012)
- [33] S.V. Shulga, S.L. Drechsler, G. Fuchs, and K.H. Müller, K. Winzer, M. Heinecke, and
K. Krug, Phys. Rev. Lett. **80**, 1730-1733 (1998); H. Suderow, V.G. Tissen, J.P. Brison,
J.L. Martinez, S. Vieira, P. Lejay, S. Lee and S. Tajima, Phys. Rev. B **70** 134518 (2004)
- [34] Y. Kamihara, T. Watanabe, M. Hirano and H. Hosono, J. Am. Chem. Soc. **130** 3296 (2008)
- [35] G.R. Stewart, Rev. Mod. Phys. **83**, 1589 (2011)

-
- [36] D. Daghero, M. Tortello, G.A. Ummarino and R.S. Gonnelli, Rep. Prog. Phys. **74**, 124509 (2011)
- [37] G.A. Ummarino, M. Tortello, D. Daghero and R.S. Gonnelli, Phys. Rev. B **80**, 172503 (2009)
- [38] D.S. Inosov, J.T. Park, P. Bourges, D.L. Sun, Y. Sidis, A. Schneidewind, K. Hradil, D. Haug, C.T. Lin, B. Keimer and V. Hinkov, Nature Phys. **6**, 178-181 (2010)
- [39] G.A. Ummarino, Phys. Rev. B **83**, 092508 (2011)
- [40] G.A. Ummarino, J. Supercond. Nov. Magn. **25**, 1333 (2012)
- [41] M. Tortello, D. Daghero, G.A. Ummarino, A.V. Stepanov, J. Jiang, J.D. Weiss, E.E. Hellstrom, and R.S. Gonnelli, Phys. Rev. Lett **105**, 237002 (2010)
- [42] P.J. Hirschfeld, M.M. Korshunov and I.I. Mazin, Rep. Prog. Phys. **74**, 124508 (2011)
- [43] L. Boeri, M. Calandra, I.I. Mazin, O.V. Dolgov and F. Mauri, Phys. Rev. B **82**, 020506R (2010)
- [44] J. Paglione and R.L. Greene, Nature Phys. **6**, 645 (2010)
- [45] G.A. Ummarino and R.S. Gonnelli, Physica C **328**, 189 (1999)
- [46] G.A. Ummarino, S. Galasso and A. Sanna, J. Phys.: Condens. Matter **25**, 205701 (2013)